Neurobiology of Disease

Intermittent Hypobaric Hypoxia Ameliorates Autistic-Like Phenotypes in Mice

Yi-da Pan,[1,2*] Yuan Zhang,[3*] Wen-ying Zheng,[2,3] Min-zhen Zhu,[2] Huan-yu Li,[2] Wen-jie Ouyang,[2,3] Qin-qing Wen,[2,4] and Xin-hong Zhu[1,2,3,4]

[1]School of Basic Medical Sciences, Southern Medical University, Guangzhou 510515, China, [2]Research Center for Brain Health, Pazhou Lab, Guangzhou 510330, China, [3]School of Psychology, Shenzhen University, Shenzhen 518060, China, and [4]School of Biology and Biological Engineering, South China University of Technology, Guangzhou 510006, China

Autism spectrum disorder (ASD) is a neurodevelopmental condition characterized by persistent deficits in social communication and stereotyped behaviors. Although major advances in basic research on autism have been achieved in the past decade, and behavioral interventions can mitigate the difficulties that individuals with autism experience, little is known about the many fundamental issues of the interventions, and no specific medication has demonstrated efficiency for the core symptoms of ASD. Intermittent hypobaric hypoxia (IHH) is characterized by repeated exposure to lowered atmospheric pressure and oxygen levels, which triggers multiple physiological adaptations in the body. Here, using two mouse models of ASD, male *Shank3B*$^{-/-}$ and *Fmr1*$^{-/y}$ mice, we found that IHH training at an altitude of 5,000 m for 4 h per day, for 14 consecutive days, ameliorated autistic-like behaviors. Moreover, IHH training enhanced hypoxia inducible factor (HIF) 1α in the dorsal raphe nucleus (DRN) and activated the DRN serotonergic neurons. Infusion of cobalt chloride into the DRN, to mimic IHH in increasing HIF1α expression or genetically knockdown PHD2 to upregulate HIF1α expression in the DRN serotonergic neurons, alleviated autistic-like behaviors in *Shank3B*$^{-/-}$ mice. In contrast, downregulation of HIF1α in DRN serotonergic neurons induced compulsive behaviors. Furthermore, upregulating HIF1α in DRN serotonergic neurons increased the firing rates of these neurons, whereas downregulation of HIF1α in DRN serotonergic neurons decreased their firing rates. These findings suggest that IHH activated DRN serotonergic neurons via upregulation of HIF1α, and thus ameliorated autistic-like phenotypes, providing a novel therapeutic option for ASD.

Key words: **autism spectrum disorder; dorsal raphe nucleus (DRN); hypoxia inducible factor (HIF) 1α; intermittent hypobaric hypoxia (IHH); serotonergic neurons**

Significance Statement

Autism spectrum disorder (ASD) affects more than 78 million individuals worldwide resulting in heavy social and economic burdens. However, no specific medication is effective for the core symptoms of ASD. Intermittent hypobaric hypoxia (IHH), a form of "living high–training low," has been used to train pilots and mountaineers. Here, we found that IHH at an altitude of 5,000 m for 4 h per day, for 14 consecutive days ameliorated autistic-like behavior in male *Shank3B* and *Fmr1* knockout mice. Moreover, IHH training increased the activation of serotonergic neurons in the dorsal raphe nucleus via upregulating HIF1α, which contributes to the anti-autistic-like effect of IHH. These findings highlight the therapeutic potential of IHH in the treatment of ASD.

Received Sept. 4, 2023; revised Nov. 27, 2023; accepted Dec. 13, 2023.

Author contributions: Y.-d.P., Y.Z., and X.-h.Z. designed research; Y.-d.P., Y.Z., W.-y.Z., M.-z.Z., H.-y.L., W.-j.O., Q.-q.W., and X.-h.Z. performed research; Y.-d.P., Y.Z., and X.-h.Z. analyzed data; Y.-d.P., Y.Z., and X.-h.Z. contributed unpublished reagents/analytic tools; Y.-d.P., Y.Z., and X.-h.Z. wrote the paper; Y.-d.P., Y.Z., and X.-h.Z. wrote the first draft of the paper; Y.-d.P., Y.Z., and X.-h.Z. edited the paper.

We thank Feng Ke, the CEO of the Eusyn Medical Tech. Co., Guangzhou, China, for providing the IHH chamber. We thank Qian-wen Zhao (Pazhou Lab), and Shu-ji Li, Ying-ying Fang, Ting Guo, Xiao-wen Li (Southern Medical University) for their technical support. This work was supported by grants from the National Natural Science Foundation of China (81930034 to X.-h.Z.), and the STI 2030 – Major project (2022ZD0211700 to X.-h.Z.).

*These authors contributed equally to this work.

The authors declare no competing financial interests.

Correspondence should be addressed to Xinhong Zhu at zhuxh527@126.com.

https://doi.org/10.1523/JNEUROSCI.1665-23.2023

Introduction

Autism spectrum disorder (ASD) is a neurodevelopmental disorder that affects more than 78 million individuals worldwide, resulting in heavy social and economic burdens (Lord et al., 2022). Major advances in basic research on autism have been achieved in the past decade, however, little is known about the fundamental issues of the interventions, and no specific medication is effective for the core symptoms of ASD (Berry-Kravis et al., 2018; Hirota and King, 2023). More efficacious therapies, particularly physical interventions, are required.

ASD is genetically heterogeneous with a heritability of 64–91%. Over 100 genes have been identified to be strongly associated with ASD, and the four largest modules are enriched in the Gene Ontology terms synapse structure and function, chromatin modification, RNA-binding proteins, and several other points of mechanistic overlap (Trost et al., 2022; Willsey et al., 2022). Intermittent hypobaric hypoxia (IHH), a form of "living high–training low," has been used to train pilots and mountaineers (Serebrovskaya and Xi, 2016). IHH is characterized by repeated exposure to lowered atmospheric pressure and oxygen levels followed by periods of normoxia and triggers multiple physiological adaptations (Neubauer, 2001). Increasing evidence indicates that IHH has the potential to treat ASD. First, IHH can promotes adult hippocampal neurogenesis, which is crucial for hippocampal functions, including spatial learning, memory, and object recognition (Zhu et al., 2010; Sun et al., 2020). Moreover, IHH training enhanced long-term potentiation in hippocampal cornu ammonis (CA) 1 slices and increased synaptic density in the CA3 of adult mice (Zhang et al., 2005). In addition, postsynaptic protein levels were increased in the hippocampus after 14 d of mild hypoxia (Lu et al., 2009). IHH training significantly increased the expression of brain-derived neurotrophic factors, which play important roles in synaptic development and plasticity in the adult hippocampus (Zhu et al., 2010; Wang et al., 2022). These results suggest that IHH affects the synaptic structure and function of the brain. Second, hypoxia inducible factor (HIF) 1α (encoded by *HIF1a*) is the central regulator of oxygen homeostasis (Bonkowsky and Son, 2018). IHH increased the expression of HIF1α and its target gene in the hippocampus of rodents (Zhu et al., 2010; Viscor et al., 2018). HIF1α recruits histone acetyltransferases, histone deacetylases, and DNA methyltransferases to modulate chromatin structure and gene accessibility (Li et al., 2021). Furthermore, HIF1α directly binds to specific DNA sequences, known as hypoxia response elements, to activate or repress the transcription of target genes (Xia et al., 2009; Semenza, 2012; Schodel and Ratcliffe, 2019). Taken together, IHH may have an extensive effect on chromatin modulation, and gene regulation via HIF1α signaling.

Mimicking core features, including repetitive movements and impaired social interaction, can be used to explore the pathogenesis of ASD and develop potential treatments (Lipkin et al., 2023). There are two types of ASD models: environmentally and genetically induced mouse models. The environmentally induced models are relevant, while the genetic models mimic ASD symptoms present in distinct human genetic diseases (Ergaz et al., 2016). A very promising ASD candidate gene is the *SHANK3*. *SHANK3* is disrupted in the Phelan-McDermid syndrome, which is characterized by systemic developmental delay and typical autistic symptoms (Herbert, 2011). *SHANK3* has three isoforms: α, β, and γ. Mice engineered to lack expression of the α and β isoforms, with reduced levels of the γ isoform, named *Shank3B*$^{-/-}$ mice, had an autism-like combination of behavioral features (Peca et al., 2011). Fragile X Syndrome is characterized by the mental retardation and autistic features and is caused by transcriptional silencing of the *FMR1* gene, culminating in the loss of the Fragile X mental retardation protein (Krueger et al., 2011; Varghese et al., 2017). Male *Fmr1* knockout (*Fmr1*$^{-/y}$) mice stably simulate the core clinical symptoms of individuals with autism (Krueger et al., 2011). In this study, using *Shank3B*$^{-/-}$ and *Fmr1*$^{-/y}$ mice, we investigated the effects of IHH on ameliorating core syndromes of ASD and the underlying mechanisms.

Materials and Methods

Animals. C57BL/6J mice (2–4 months old) were obtained from the Southern Medical University Animal Center (Guangzhou, China). The following strains of transgenic mice were purchased from Jackson Laboratory: *Shank3B*$^{-/-}$ mice, JAX stock 017688, RRID: IMSR_JAX:017688; *Fmr1*$^{-/y}$ mice, JAX stock 003025, RRID: IMSR_JAX:003025; *ePet1*-Cre mice, JAX stock 012712, RRID: IMSR_JAX:012712; and Ai9 (Rosa26-tdTomato reporter) mice, JAX stock 007909, RRID: IMSR_JAX:007909. We generated *Shank3B*$^{-/-}$; *ePet1*-Cre mice by crossing *Shank3B*$^{-/-}$ mice with *ePet1*-Cre mice, generated *ePet1*^{tdtomato} mice by crossing *ePet1*-Cre mice with Ai9 mice. All mice had a C57BL/6J background and were housed in standard plastic rodent cages under standard laboratory conditions (24°C, 12 h/12 h light/dark cycle [lights on at 07:00 h]), with free access to food and water. Only male mice were used in the experiments. All behavioral tests in a conducted double-blinded manner, and before the behavioral experiments, the mice were handled twice a day for at least successive three days. All the experiments were conducted in accordance with the Chinese Council on Animal Care guidelines.

IHH training protocol. IHH training was performed as we previously described protocol (Zhu et al., 2010). Briefly, 6-week-old mice were placed inside a specially designed hypoxic chamber (Eusyn Medical Tech. Co., Guangzhou, China, Fig. 1). To gradually reduce the oxygen levels, a computer program controlled the vacuum pump system, simulating a gradual descent from atmospheric pressure (21% O_2) to a partial pressure of 10% O_2, which corresponds to an altitude of approximately 5,000 m. The progressive decrease in oxygen tension lasted for

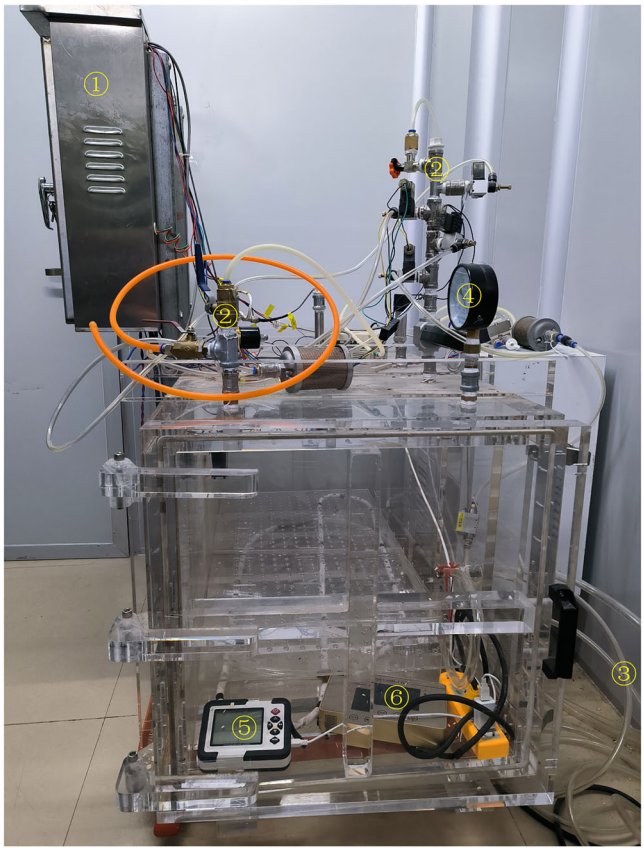

Figure 1. IHH chamber. The intermittent hypobaric hypoxia chamber is primarily composed of a chamber body made of organic glass (130 × 80 × 80 cm), a vacuum compression pump system, and a computer control system, which can simulate a gradual descent from atmospheric pressure to the target partial pressure of oxygen. ① Computer monitor, ② Air-intake duct, ③ Vacuum-pumping pipeline, ④ Barometer, ⑤ CO_2 monitor, ⑥ O_2 monitor.

approximately 30 min. Subsequently, the mice were exposed to a partial pressure of 10% O_2 for 4 h. Next, the oxygen levels inside the chamber were restored back to normal atmospheric pressure over a period of 30 min, and after which the mice were returned to their home cages. The experiment was performed at the same time, once daily for 14 consecutive days, and the chamber was cleaned daily. For normoxic controls, mice were kept in their home cages with circulating room air for 4 h during the corresponding period.

Grooming test. A grooming experiment was conducted between 19:00 (the onset of the dark cycle) and 21:00, as previously described (Kalueff et al., 2007). Mice were placed in a white plexiglass chamber (20 × 20 × 30 cm), and after 10 min of habituation, their behavior was video-recorded for 10 min. A stopwatch was used to calculate the grooming time, including head washing, body grooming, genital/tail grooming, and paw and leg licking.

Marble burying test (MBT). The marble burying test (MBT) was conducted as a previous report (Dhamne et al., 2017). Briefly, the MBT was conducted between 09:00 and 16:00 using a standard plastic cage (26 × 48 × 20 cm) with a lid. Fresh unscented bedding (5 cm) was added to the cages and pressed flat. Subsequently, 20 marbles (diameter 15 mm, 5.2 g, various colors; cleaned with detergent and dried before use) were placed in the cage, which was divided into five rows of four marbles each. The mice were individually placed in a corner of the cage containing the marbles, as far from the marbles as possible. The lid was then closed and each mouse was allowed to freely explore the cage for 30 min. Next, each mice was carefully removed from the cage, taking care not to touch the marbles during trapping. Marbles covered by at least two-thirds of bedding were scored as buried.

Three-chamber sociability test. The three-chamber sociability test was performed as previously described (Rein et al., 2020). The test apparatus consisted of a middle chamber (20 × 40 × 20 cm) and two side chambers (20 × 40 × 20 cm each) in which wire cages containing stranger mice were placed. For the social preference test, the test animal was placed in the chamber for 10 min for habituation. A wire cage containing a novel adult male mouse (Stranger 1, S1) of the same age was placed in one side chambers, and an empty wire cage was placed in the other side chambers. For the social novel preference test, another novel adult male mouse (Stranger 2, S2) of the same age was placed in the empty cage. The original stranger mouse (S1) having been in contact with the experimental mouse for some time and was thus relatively familiar with it. The time spent in each chamber and the time spent close to the wire cages were analyzed using Ethovision XT 11.5 software (Nodlus Information Technology, Netherlands).

Y-maze test. The Y-maze apparatus was made of gray plexiglass, and had three identical 30 × 10 × 20 cm arms with a central area connected to the three arms by a 10 × 10 × 10 cm triangle. Each arm formed a 120° angle with the other two arms. During the experiment, mice were placed in the central area to explore the maze freely for 5 min. The order in which the mice entered the arms was recorded. Consecutive choices of three different arms counted as alternate choices and scored one point. The total number of opportunities for alternation was calculated as the total number of arm entries minus two. Percentage correct rate = (total alternation points/total alternation opportunities) × 100.

Brain tissue collection. Mice were euthanized by cervical dislocation, and the brains were rapidly removed and placed in ice-cold phosphate-buffered saline (PBS). Brain slices (0.5 mm in thickness) containing the medial prefrontal cortex (mPFC) (Bregma: 1.34–2.34 mm), nucleus accumbens (NAc) (Bregma: 0.74–1.94 mm), striatum (Bregma: 0.02–1.54 mm), amygdala (Bregma: −1.70 – −0.70 mm), dorsal raphe nucleus (DRN) (Bregma: −4.96 – −4.24 mm) were carefully excised using a brain matrix (catalog #68713, RWD Life science, Shenzhen, China) for precise sectioning. The coordinates for brain region collection were determined based on established mouse brain atlas references (Paxinos and Franklin, 2004; Kim et al., 2018).

Nuclear and cytoplasmic fractionation. The DRN nuclear/cytoplasmic protein extracts were prepared according to the manufacturer's guidelines (catalog #78833; ThermoFisher Scientific, USA), and endogenous Lamin B1 and β-actin were used as the makers for the purification of the nucleus and cytoplasm, respectively.

Immunoblotting analysis. Total protein was extracted from tissues using RIPA lysis buffer (catalog #P0013B; Beyotime, Shanghai, China) containing a protease inhibitor (catalog #ST506-2; Beyotime). Protein concentrations in the lysate supernatants were measured using a BCA kit (catalog #23225, ThermoFisher Scientific). For western blot, samples containing 60 μg of total protein were loaded onto sodium dodecyl sulfate polyacrylamide gels. The stacking gel (5% concentration) was used for sample loading, whereas a separation gel (10% concentration) facilitated the separation of proteins. Subsequently, the separated proteins were transferred onto polyvinylidene difluoride membranes. Following the transfer, the membranes were blocked with skim milk for a duration of 1 h. The membranes were thoroughly washed with Tris-buffered saline containing Tween 20 solution, with three cycles of 5-min washes. Next, the membranes were incubated overnight at 4°C with continuous agitation in primary antibodies. After incubation with the primary antibody, peroxidase-conjugated secondary antibodies (Peroxidase-Conjugated AffiniPure Goat Anti-Rabbit/Mouse IgG [H + L], ZSGB-Bio, Beijing, China) were applied for 1 h incubation. Protein bands on the membranes were visualized using Western Lightning ECL (PerkinElmer, Waltham, MA, USA). The following primary antibodies were used for the western blot analysis: Rabbit anti-GluR1 (1:10,000, catalog #ab31232, RRID: AB_2113447, Abcam, USA), Rabbit anti-GluR2 (1:10,000, catalog #ab133477, RRID: AB_2620181, Abcam, USA), Rabbit anti-NR2A (1:1,000, catalog #4205, RRID: AB_2112295, Cell Signaling Technology, USA), Rabbit anti-NR2B (1:1,000, catalog #4207, RRID: AB_1264223, Cell Signaling Technology, USA), and Rabbit anti-GAPDH (1:5,000, catalog #10494-1-AP, RRID: AB_2263076, Proteintech, USA). The protein levels were normalized to GAPDH on the same gel. All quantification was performed with AlphaEaseFC software (Alpha Innotech Corporation, USA).

The JESS system (Bio-Techne; ProteinSimple, San Jose, CA, USA) was used for Simple Western assay. The relative amount of each protein was quantified *via* the peak areas detected in the chemiluminescence electropherogram generated by the Compass for Simple Western software (ProteinSimple, San Jose, CA, USA). The following primary antibodies were used for the Simple Western assay analysis: rabbit anti-HIF1α (1:50, catalog #14179S, RRID: AB_2622225, Cell Signaling Technology, USA); rabbit anti-PHD2 (1:200, catalog #NB100-2219, RRID: AB_2096717, Novus Biological, USA), rabbit anti-β-actin (1:200, catalog #20536-1-AP, RRID: AB_10700003, Proteintech, USA), rabbit anti-Lamin B1 (1:150, catalog #ab16048, RRID: AB_443298, Abcam, USA), rabbit anti-GluR1 (1:5,000, catalog #ab31232, RRID: AB_2113447, Abcam, USA), rabbit anti-GluR2 (1:5,000, catalog #ab133477, RRID: AB_2620181, Abcam, USA), rabbit anti-NR2A (1:200, catalog #4205, RRID: AB_2112295, Cell Signaling Technology, USA), rabbit anti-NR2B (1:200, catalog #4207, RRID: AB_1264223, Cell Signaling Technology, USA). The protein levels were normalized to β-actin.

Immunohistochemistry. Mice were anesthetized with pentobarbital (intraperitoneally, 75 mg/kg) and perfused with saline followed by 4% paraformaldehyde. The brains were carefully removed, post-perfused with 4% paraformaldehyde for 24 h, and immersed in 30% sucrose solution. Coronal brain slices (40-μm thick) encompassing the mPFC (Bregma: 1.34–2.34 mm), NAc (Bregma: 0.74–1.94 mm), amygdala (Bregma: −1.70 – −0.70 mm), hippocampus (Bregma: −2.80 – −1.34 mm), ventral tegmental area (VTA) (Bregma: −3.88 – −2.92 mm), and DRN (Bregma: −4.96 – −4.24 mm) were obtained using a freezing microtome (CM1950; Leica Microsystems, Wetzlar,

Germany). One of every four consecutive slices from the regions of interest was selected for immunostaining (mPFC, six slices; NAc, eight slices; amygdala, six slices; hippocampus, nine slices; VTA, six slices; DRN, five slices; for each brain area). Free-floating sections were washed 3 × 5 min with PBS, permeabilized in PBS containing 0.3% Triton X-100 for 30 min, blocked in 5% normal goat serum solution containing 0.3% Triton X-100 for 2 h at room temperature, and incubated with primary antibody overnight at 4°C. The primary antibodies used were rabbit anti-TPH2 (1:300, catalog #NB100-74555, RRID: AB_1049988, Novus Biologicals, USA), mouse anti-TPH2 (1:300, catalog #T0678, RRID: AB_261587, Sigma-Aldrich, USA), rabbit anti-c-Fos (1:500, catalog #2250, RRID: AB_2247211, Cell Signaling Technology, USA), mouse anti-HIF1α (1:50, catalog #NB100-105, RRID: AB_350048, Novus Biological, USA), and rabbit anti-NeuN (1:500, catalog #MABN140, RRID: AB_257156, Millipore, USA). After washing, the sections were incubated with secondary antibodies (1:500, catalog #A21206, RRID: AB_2535792, donkey anti-rabbit IgG [H + L] Alexa Fluor 488; catalog #A10042, RRID: AB_2534017, donkey anti-rabbit IgG [H + L] Alexa Fluor 568; catalog #A10037, RRID: AB_11180865, donkey anti-mouse IgG [H + L] Alexa Fluor 568; Invitrogen, Waltham, MA, USA) for 2 h and mounted with mounting medium containing diamidinophenyl-indole (Vectashield; Vector Laboratories, Burlingame, CA, USA).

Cell counts and fluorescence intensity measurement. Brain slices were imaged using an inverted Nikon confocal microscope (A1; Nikon, Japan). For immunopositive cell counting, the imaris surface mode was used to construct the surface of the region, and all immunopositive cells were quantified using an automatic spot-detection algorithm within the surface of the region (Imaris 9.7.1, Bitplane AG). After counting the positive cells in each slice, the total number of immunopositive cells for each animal in a specific brain region was calculated and normalized to their corresponding controls.

HIF1α fluorescence intensity was measured for both control and experimental image sets, which were captured using identical imaging parameters (e.g., laser intensity, gain). Quantification of HIF1α fluorescence intensity was performed by calculating the mean fluorescence pixel intensity using Image J (version 1.54, NIH). Relative HIF1α fluorescence intensity was calculated and normalized to their corresponding controls.

Quantitative real-time PCR (qPCR). Total RNA was extracted using the RNAiso reagent according to the manufacturer's instructions (catalog #9109, TaKaRa Bio, Tokyo, Japan), and reverse transcribed into cDNA using PrimeScript RT Master Mix (catalog #RR047A, TaKaRa Bio). Quantitative PCR was performed using the TB Green qPCR Master Mix (catalog #RR420A, TaKaRa Bio). The18S ribosomal RNA was used as the internal control for normalization. The sequences of the primers used in this study were *Hif1a*: 5′-CGCCTCTGGAC TTGTCTCTTT-3′ and 5′-TTCGACGTTCAGAACTCATCC-3′; and *18S*: 5′-AGTTCCAGCACATTTTGCGAG-3′ and 5′-TCATCCTCC GTGAGTTCTCCA -3′.

Virus production. The recombination adeno-associated virus (rAAV)2/9-CMV-Cre-hGH-pA (titer: 5.54×10^{12} vg/ml) and rAAV2/9-EF1α-DIO-GCaMP6f-WPRE-hGH-pA (titer: 3.06×10^{12} vg/ml) were purchased from BrainVTA (Wuhan, China). To knockdown *Engl1,* which encodes prolyl hydroxylase domain-containing protein 2 (PHD2), rAAV2/9-hEF1a-DIO-EGFP-*Egln1*-shRNA (titer: 3.70×10^{13} vg/ml) was purchased from Shanghai Taitool Bioscience (Shanghai, China), and the shRNA sequence was 5′-GCATGAACAA GCACGGCATCT-3′. For *Hif1α* knockdown, the shRNA sequence was 5′-CCAGTTACGATTGTGAAGTTA-3′, and rAAV2/9-CBG-DIO-EGFP-*Hif1a*-shRNA (titer: 6.56×10^{12} vg/ml) was produced by Obio Technology (Shanghai, China). rAAV-hEF1a (or CBG)-DIO-scrambled sequence-EGFP (SC) (titer: 6.56×10^{12} vg/ml) was used as a control virus.

Virus injection and optical fiber/cannula implantation. Mice were anesthetized and placed on a stereotaxic frame (RWD Life science, Shenzhen, China). The virus was injected using a micro-syringe pump (Stoelting, Wood Dale, IL, USA) fitted with a 33-gauge needle at a rate of 0.1 μl/min. After injection, the cannula was left at the injection site for 10 min and then slowly removed. Viruses were injected into the DRN of *ePet1*-Cre mice to modulate gene expression in the DRN serotonergic neurons. The injection coordinates and volumes used (mediolateral [ML], anterioposterior [AP], and dorsoventral [DV] coordinates relative to the bregma) are as follows: ML = +0.83 mm, AP = −4.60 mm, DV = −3.18 mm; total volume 500 nl (a 15° angle from the caudal to rostral region). For fiber photometry, after virus injection, mice received a surgical implantation of a ceramic ferrule (200 μm; Inper, Hangzhou, China) above the DRN. For pharmacological experiments, a unilateral cannula (RWD Life Science) was implanted above the DRN for the infusion of $CoCl_2$ (catalog #232696, Sigma-Aldrich, 200 μM, total volume 1 μl) or artificial cerebrospinal fluid (ACSF) containing 126 mM NaCl, 26 mM $NaHCO_3$, 3 mM KCl, 1.25 mM NaH_2PO_4, 2 mM $CaCl_2$, 1 mM $MgSO_4$, and 10 mM D-glucose. The cannula was held in place with dental cement. A stainless steel obturator was inserted into each guide cannula to prevent blockage. Only mice with optical fibers/cannulas and viral expression at the correct locations were used for further analysis.

Fiber photometry recording. Photometric recordings were conducted using the fiber photometry recording system (QAXK-FPS-TC-LED, Thinkerbiotech, Nanjing, China) three weeks after optical fiber implantation. To record fluorescence signals, two laser beams from the laser tube (405 nm and 470 nm) were reflected by a dichroic mirror focused by a 10× objective (NA 0.3) and coupled to an optical commutator. To minimize photobleaching, the laser power at the fiber tip was adjusted to 30 μW. For recordings in mice, the fluorescence signals from mice with optical fibers connected to the fiber photometry system were recorded during the IHH. Bulk fluorescence signals were acquired and analyzed with MATLAB software (version R2018a, MathWorks, USA). The 405 nm signal was scaled using least-squares regression and then subtracted from the 470 nm signal to generate the corrected 470 nm signal. The Ca^{2+} transient rate, ΔF/F (%), was calculated as the average change in fluorescence during the IHH: $\Delta F/F\ (\%) = (V_{signal} - F_0)/(F_0 - V_{offset}) \times 100$, $F_0 = \overline{v_{basal}}$, which V_{basal} was defined as the reference basal time (1-min prior to each IHH phase).

In vitro *electrophysiological recording.* Mice (8–14 weeks old) were deeply anesthetized and rapidly decapitated. The brains were removed from the cranial cavity and dissected into an ice-cold cutting solution containing 195 mM sucrose, 2 mM KCl, 0.2 mM $CaCl_2$, 12 mM $MgSO_4$, 1.3 mM NaH_2PO_4, 26 mM $NaHCO_3$, and 10 mM D-glucose. Coronal brain sections (300-μm thick) containing DRN were cut using a vibratome (VT-1200S, Leica, Germany). Brain slices were incubated at 34°C for 30 min and then at room temperature (25 ± 1°C) for recovery in a holding chamber containing ACSF before being transferred to the recording chamber for electrophysiological recordings. All solutions were saturated with 95% O_2/5% CO_2 (*vol*/*vol*).

Electrophysiological recordings were performed using a MultiClamp 700B amplifier and pClamp software (Molecular Devices, USA). The data were low-pass filtered at 3 kHz and digitized at 10 kHz using Digidata 1550B (Molecular Devices, USA). During the recording, the slices were submerged in normal oxygenated ACSF and superfused (2 ml/min) at a temperature of 32–34°C. A pipette (4–6 MΩ) was pulled using a micropipette puller (PC-100 Narishige, Japan) and filled with an internal solution containing 130 mM K-D-gluconate, 20 mM KCl, 10 mM HEPES, 10 mM phosphocreatine, 4 mM ATP-Mg, 0.3 mM GTP-Na and 0.2 mM EGTA (pH 7.32, 299 mOsm). Neurons were held at −70 mV during seal formation and breaking the cell member. Spontaneous firing activity of the serotonergic neurons were recorded in cell-attached voltage clamp or current-clamp mode without holding ($I = 0$) and the spontaneous firing rate was measured as the average firing frequency from a 2-min recording. To induce an action potential in DRN serotonergic neurons, whole-cell recordings were performed in current-clamp mode. The action potential parameters were measured from responses to depolarizing current steps (−50 to +350 pA, 300 ms or −30 to +160 pA, 500 ms), with the neurons held at −70 mV. The

distinctive features of the action potential in each cell were identified by analyzing the initial action potential evoked in response to depolarizing steps. All recordings were excluded if the holding current exceeded −100 pA or if series resistance was greater than 30 MΩ or fluctuated by more than 20% from the initial values. Data were acquired using pClAMP 10.7 and analyzed using Clampfit 10.7 software.

Quantification and statistical analysis. All data were analyzed using GraphPad Prism 9.3.1 (GraphPad Software, San Diego, CA, USA), and are presented as means ± standard error of the mean (SEM). Statistical differences between two populations were calculated by *t* test (2-tailed) including multiple *t* test and unpaired Student's *t* test. For comparisons among three or more groups, a one-way ANOVA was used, followed by the least significant difference test (when equal variances were assumed) or Dunnett's T3 test (when equal variances were not assumed) for post hoc comparisons. Two-way ANOVA followed by Bonferroni's multiple-comparisons test was used for repeated measures. Differences were considered statistically significant if $p < 0.05$.

Results

IHH ameliorated autistic-like phenotypes in *Shank3B*$^{-/-}$ mice

Disruption of *SHANK3* is linked to ASD in humans and leads to social impairments in macaques (Zhou et al., 2019). Consistently, *Shank3B*$^{-/-}$ mice display repetitive behaviors and social deficits (Peca et al., 2011), two core syndromes of ASD. To investigate the effect of IHH on autistic-like behaviors, we first subjected *Shank3B*$^{-/-}$ mice and their littermate controls, *Shank3B*$^{+/+}$ mice, to IHH for 14 consecutive days. Next they were subjected to the grooming and three-chamber sociability tests, which are commonly used to assessed repetitive behaviors and sociability in animal models of ASD (Kazdoba et al., 2016), respectively (Fig. 2*A*). *Shank3B*$^{-/-}$ mice showed signs of overgrooming, compared with *Shank3B*$^{+/+}$ mice. This result is consistent with that of a previous study (Peca et al., 2011). The grooming time in *Shank3B*$^{-/-}$ mice was significantly decreased following IHH training, compared to that of *Shank3B*$^{-/-}$ mice under the normoxic conditions, whereas a little effect of IHH on grooming was observed in *Shank3B*$^{+/+}$ mice (Fig. 2*B*; $F_{(1,77)} = 7.3220$, $p = 0.0084$, interaction, $F_{(1,77)} = 1.9670$, $p = 0.1648$, two-way ANOVA). In the three-chamber test, the mice were successively tested in two phases: social preference and social novelty tests after 10 min of habituation. For the social preference test, mice were allowed to interact with a mouse (S1) or an empty cup; *Shank3B*$^{+/+}$ mice preferred to interact with the S1 mouse, whereas *Shank3B*$^{-/-}$ mice spent similar amounts of time interacting with the S1 mouse and the empty cup. However, after IHH training, *Shank3B*$^{-/-}$ mice behaved similarly to their

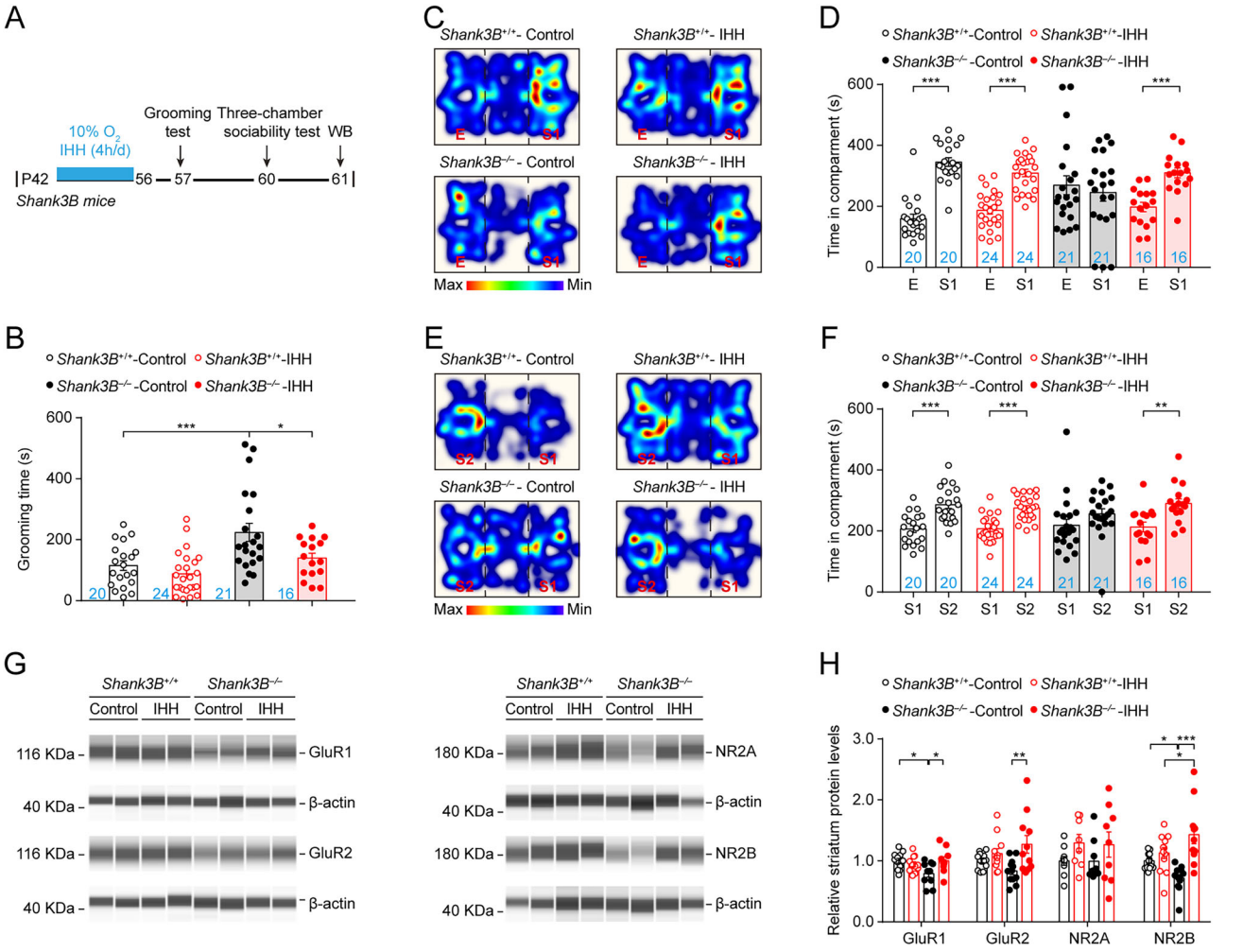

Figure 2. IHH ameliorated autistic-like phenotypes in *Shank3B*$^{-/-}$ mice. ***A***, Experimental protocol. WB, western bolt; P42, postnatal day 42. ***B***, Grooming time in each group following treatment with or without IHH ($n = 16$–24 mice per group). ***C–F***, Representative heat maps and statistics for the three-chamber sociability test. IHH treatment improved the social preference (***C, D***) and social novelty abilities (***E, F***) in *Shank3B*$^{-/-}$ mice ($n = 16$–24 mice per group). ***G***, Representative bands of western blot. ***H***, Protein levels of GluR1, GluR2, NR2A, and NR2B in the striatum of *Shank3B*$^{-/-}$ and control mice following IHH ($n = 6$–8 mice per group). Data are presented as mean ± SEM. *$p < 0.05$, **$p < 0.01$, ***$p < 0.001$.

control littermates, displaying a stronger preference for the S1 mouse (Fig. 2C,D; *Shank3B*$^{+/+}$-Control: $F_{(2,57)} = 103.8530$, $p < 0.0001$; *Shank3B*$^{+/+}$-IHH: $F_{(2,69)} = 105.7710$, $p < 0.0001$; *Shank3B*$^{-/-}$ -Control: $F_{(2,60)} = 20.1010$, $p < 0.0001$; *Shank3B*$^{-/-}$-IHH: $F_{(2,45)} = 64.8580$, $p < 0.0001$, one-way ANOVA). To examine the effect of IHH on social novelty behavior, we replaced the empty cup with an S2 mouse and calculated the duration of the interaction with S1 and S2. While control littermates spent more time interacting with S2 than with S1, *Shank3B*$^{-/-}$ mice spent equal time interacting with S1 and S2, indicating that *Shank3B*$^{-/-}$ mice exhibited deficits in the social novelty preference. Notably, the social deficits seen in *Shank3B*$^{-/-}$ mice were reversed after IHH training (Fig. 2E,F; *Shank3B*$^{+/+}$-Control: $F_{(2,57)} = 71.7870$, $p < 0.0001$; *Shank3B*$^{+/+}$-IHH: $F_{(2,69)} = 103.4510$, $p < 0.0001$; *Shank3B*$^{-/-}$-Control: $F_{(2,60)} = 22.2950$, $p < 0.0001$; *Shank3B*$^{-/-}$-IHH: $F_{(2,45)} = 52.9920$, $p < 0.0001$, one-way ANOVA). These results suggest that IHH ameliorates autistic-like behaviors in *Shank3B*$^{-/-}$ mice.

SHANK3 encodes a key postsynaptic density (PSD) protein at glutamatergic synapses, and the striatum has been strongly implicated in autism-associated behaviors (Peca et al., 2011; DiCarlo et al., 2019; Li and Pozzo-Miller, 2020). Therefore, we assessed whether IHH training affects postsynaptic protein levels in the striatum. Glutamate receptor 1 (GluR1) and N-methyl-d-aspartate receptor subunit 2A (NR2A) levels significantly decreased in the striatum of *Shank3B*$^{-/-}$ mice, whereas the glutamate receptor 2 (GluR2) protein level was slightly decreased compared to that in control littermates, which is generally in agreement with a previous study (Peca et al., 2011). We found that IHH training reversed the decreased levels of the GluR1, GluR2, and N-methyl-d-aspartate receptor subunit 2B (NR2B) proteins in *Shank3B*$^{-/-}$ mice, while IHH had little effect on the expression of these PSD proteins in *Shank3B*$^{+/+}$ mice (Fig. 2G,H; GluR1: $F_{(1,39)} = 2.3440$, $p = 0.1338$, interaction, $F_{(1,39)} = 6.9710$, $p = 0.0119$; GluR2: $F_{(1,45)} = 11.3100$, $p = 0.0016$, interaction, $F_{(1,45)} = 3.7080$, $p = 0.0605$; NR2A: $F_{(1,32)} = 4.0990$, $p = 0.0513$, interaction, $F_{(1,32)} = 0.0053$, $p = 0.9425$; NR2B: $F_{(1,45)} = 23.1300$, $p < 0.0001$, interaction, $F_{(1,45)} = 11.2300$, $p = 0.0016$, two-way ANOVA). Taken together, these results indicate that IHH ameliorated the autistic phenotypes in *Shank3B*$^{-/-}$ mice.

IHH improved compulsive behaviors in *Fmr1*$^{-/y}$ mice

FMR1 is highly conserved between humans and mice (Ashley et al., 1993). The *FMR1* is a single gene on the X chromosome, and male *Fmr1*$^{-/y}$ mice are the most commonly used genetic mouse models for ASD (Darnell et al., 2011; Hagerman et al., 2017). While *Fmr1*$^{-/y}$ mice display repetitive behavior, they do not exhibit repetitive self-grooming; instead, they display high levels of marble burying, which is another behavioral paradigm used to detect repetitive behavior (Barbosa-Silva et al., 2022). To further characterize the effect of IHH training on alleviating autistic-like behaviors, we subjected *Fmr1*$^{-/y}$ mice to a 14-day IHH training and the MBT was conducted 1 d after the training (Fig. 3A). Behavioral tests showed that *Fmr1*$^{-/y}$ mice buried more marbles than their wild-type littermates, *Fmr1*$^{+/y}$ mice. In contrast, IHH training significantly decreased the number of marbles buried by *Fmr1*$^{-/y}$ mice, compared to that of their knockout littermates (Fig. 3B; $F_{(1,103)} = 11.3900$, $p = 0.0010$, interaction, $F_{(1,103)} = 3.7200$, $p = 0.0565$, two-way ANOVA). Previous studies have shown that *Fmr1*$^{-/y}$ mice exhibited cognitive impairments (Bilousova et al., 2009; Zhang et al., 2017) and that IHH has the potential to enhance cognitive function (Zhang et al., 2005). Therefore, we performed the Y-maze test. However, we observed no significant differences between the groups (Fig. 3C; $F_{(1,54)} = 0.4839$, $p = 0.4896$, interaction, $F_{(1,54)} = 0.0261$, $p = 0.8723$, two-way ANOVA), possibly because of the different genetic backgrounds of the mice used.

Synaptic disruption was observed in the mPFC of *Fmr1*$^{-/y}$ mice (Krueger et al., 2011). Therefore, we examined the PSD protein levels in the mPFC of *Fmr1*$^{-/y}$ mice, and found that the

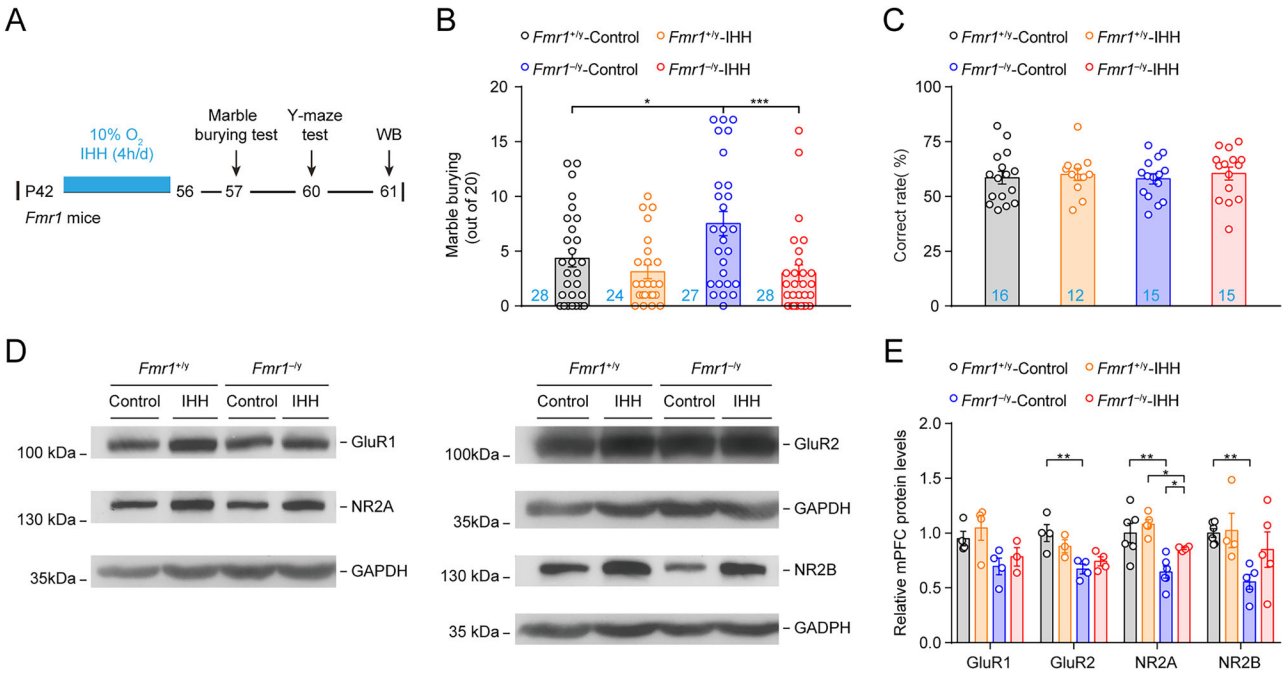

Figure 3. IHH improved compulsive behaviors in *Fmr1*$^{-/y}$ mice. ***A***, Experimental protocol. WB, western bolt; P42, postnatal day 42. ***B***, Statistical data in the marble burying test ($n = 24$–28 mice per group). ***C***, Correct rate in the Y-maze test ($n = 12$–16 mice per group). ***D, E***, Western blot analysis for GluR1, GluR2, NR2A, and NR2B expression in the medial prefrontal cortex in *Fmr1*$^{-/y}$ mice and control littermates ($n = 3$–6 mice per group). Data are presented as mean ± SEM. *$p < 0.05$, **$p < 0.01$, ***$p < 0.001$.

protein levels of GluR2, NR2A, and NR2B were significantly lower in the mPFC of *Fmr1*$^{-/y}$ mice than that of their wild-type littermates. Intriguingly, IHH training partially reversed the decreased protein levels of NR2A and NR2B in the mPFC of *Fmr1*$^{-/y}$ mice; however, IHH had little effect on the expression of GluR1 and GluR2 (Fig. 3*D*,*E*; GluR1: $F_{(1,11)} = 1.0930$, $p = 0.3182$, interaction, $F_{(1,11)} = 0.0032$, $p = 0.9559$; GluR2: $F_{(1,11)} = 0.1802$, $p = 0.6794$, interaction, $F_{(1, 11)} = 2.6800$, $p = 0.1299$; NR2A: $F_{(1,17)} = 5.3310$, $p = 0.0338$, interaction, $F_{(1,17)} = 1.0840$, $p = 0.3123$; NR2B: $F_{(1,16)} = 2.1020$, $p = 0.1664$, interaction, $F_{(1,16)} = 1.5040$, $p = 0.2378$, two-way ANOVA). Taken together, these results suggest that IHH training ameliorated autistic-like phenotypes in *Fmr1*$^{-/y}$ mice.

IHH increased the expression of HIF1α in the DRN

To investigate the mechanism underlying the effect of IHH training on alleviating autistic-like phenotypes, we first performed immunohistochemistry for c-Fos, a marker of neuronal activation (Herrera and Robertson, 1996; Russo et al., 2012), on brain slices collected from C57BL/6J mice with or without IHH training. Brain areas including the mPFC, NAc, basolateral amygdala (BLA), central nucleus of the amygdala (CeA), dentate gyrus (DG), CA1 and CA3 of the hippocampus, VTA, and DRN were examined because these brain regions are thought to be involved in neuropsychiatric disorders (Russo et al., 2012). No change was observed in the number of c-Fos-positive cells in these brain areas except the mPFC and DRN following IHH training, compared to their corresponding controls (Fig. 4*A*,*B*; mPFC: $t_{(8)} = 3.9470$, $q = 0.0206$; NAc: $t_{(4)} = 1.2160$, $q = 0.0529$; BLA: $t_{(4)} = 0.6593$, $q = 0.8019$; CeA: $t_{(4)} = 1.5570$, $q = 0.5288$; DG: $t_{(4)} = 1.4020$, $q = 0.5288$; CA1: $t_{(4)} = 0.2706$, $q = 0.9091$; CA3: $t_{(4)} = 0.0337$, $q = 0.9845$; VTA: $t_{(4)} = 0.5405$, $q = 0.8019$; DRN: $t_{(8)} = 3.9020$, $q = 0.0206$, multiple *t*-test).

HIF1α is the key cellular regulator in the hypoxia response (Baik and Jain, 2020). To further investigate which brain region contributes to the effect of IHH, we examined the expression of *Hif1a* in the mPFC, DRN, NAc, amygdala, and striatum using qPCR, and found that the mRNA level of *Hif1a* significantly increased only in the DRN (Fig. 4*C*; mPFC: $t_{(10)} = 1.9900$, $q = 0.1508$; striatum: $t_{(10)} = 0.9149$, $q = 0.3085$; NAc: $t_{(10)} = 0.9149$, $q = 0.3085$; amygdala: $t_{(10)} = 0.9736$, $q = 0.3085$; DRN: $t_{(10)} = 5.3750$, $q = 0.0013$, multiple *t*-test). This result was validated by immunostaining with anti-HIF1α antibody, showing that the fluorescence intensity of HIF1α significantly increased in the DRN, not in the mPFC (Fig. 4*D*,*E*; mPFC: $t_{(4)} = 1.7290$, $p = 0.159$; DRN: $t_{(4)} = 6.2020$, $p = 0.0034$, unpaired Student's *t* test). To determine whether HIF1α enters the nucleus, we performed western blot assay. Consistently, we found that the protein level of HIF1α significantly increased in the DRN after the 14-day IHH training. Both cytoplasmic and nuclear levels of HIF1α were higher than that of the controls (Fig. 4*F*–*I*; homogenate: $t_{(8)} = 2.4240$, $p = 0.0416$; cytoplasm: $t_{(14)} = 2.5900$, $p = 0.0214$; nucleus:

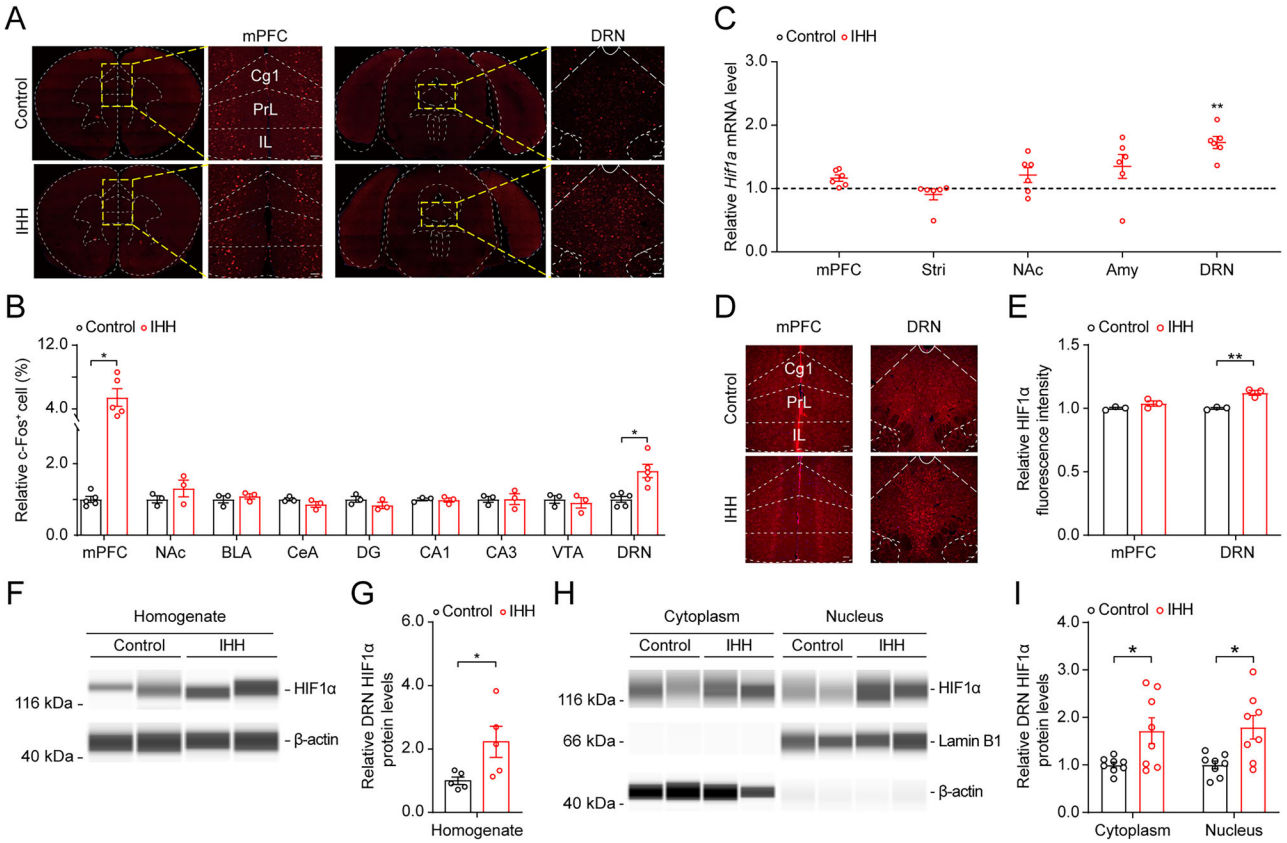

Figure 4. IHH enhanced HIF1α signaling in the DRN of C57BL/6J mice. ***A***, Representative images of c-Fos-positive cells in the medial prefrontal cortex (mPFC) and the dorsal raphe nucleus (DRN). Cg1, cingulate cortex, area 1; PrL, prelimbic cortex; IL, infralimbic cortex. ***B***, Relative number of c-Fos-positive cells in different brain regions ($n = 3$–5 mice per group). NAc, nucleus accumbens; BLA, basolateral amygdala; CeA, central nucleus of the amygdala; DG, dentate gyrus; VTA, ventral tegmental area. ***C***, Relative levels of *Hif1a* in different brain regions ($n = 6$ mice per group). Stri, striatum; Amy, Amygdala. ***D, E***, Relative fluorescence intensity of HIF1α in the mPFC and DRN of mice treated with or without IHH ($n = 3$ mice per group). ***F–I***, Representative western blot bands and statistics of HIF1α protein levels in the DRN (cytoplasm and nucleus parts) of C57BL/6J mice treated with or without IHH ($n = 5$–8 mice per group). Scale bar = 50 μm. Data are presented as mean ± SEM. $^*p < 0.05$, $^{**}p < 0.01$, $^{***}p < 0.001$.

$t_{(14)} = 3.0450$, $p = 0.0087$, unpaired Student's t test). These data indicated that HIF1α-mediated adaptations in the DRN contributes to the anti-autistic-like effect of IHH.

IHH activated serotonergic neurons in the DRN

The DRN is the predominant source of serotonergic innervation in the forebrain and is closely related to social and compulsive behaviors (Goddard et al., 2008; Walsh et al., 2018). To investigate the effect of IHH on serotonergic neurons in the DRN, we performed co-staining with anti-tryptophan hydroxylase (Tph2), a serotonergic neuron-specific marker (Jacobsen et al., 2012), and anti-c-Fos antibodies. Again, we observed a marked increase in the number of c-Fos-positive cells in the DRN following the IHH training. Intriguingly, the number of neurons with dual expression of c-Fos and Tph2 was approximately three-fold higher in the DRN of mice treated with IHH than that of control animals (Fig. 5*A*, B; c-Fos: $t_{(4)} = 3.270$, $p = 0.0308$; c-Fos/Tph2 co-staining: $t_{(4)} = 7.5530$, $p = 0.0016$, unpaired Student's t test). This indicated that IHH activated the serotonergic neurons in the DRN, contributing to the anti-autistic-like effect of IHH. Previous reports have shown that optogenetic activation of DRN serotonin neurons rescued sociability deficits (Luo et al., 2017; Walsh et al., 2018). To verify our hypothesis, we crossed *ePet1*-Cre mice, in which recombined Cre was expressed in raphe serotonergic neurons (Scott et al., 2005), with *Ai9-tdTomato* reporter mice to label serotonergic neurons in the DRN (referred as DRN^{ePet1} neurons) (Liu et al., 2014). Moreover, we examined the electrophysiological properties of DRN^{ePet1} neurons after 14 d of IHH training using whole-cell patch-clamp recordings in acute DRN slices. We found that IHH significantly increased the firing rate of DRN^{ePet1} neurons but decreased the amplitude and spike half-width of the action potentials (Fig. 5*C*; Frequency: $F_{(1,51)} = 6.3460$, $p = 0.0149$, two-way ANOVA; amplitude: $t_{(51)} = 2.5800$, $p = 0.0128$; half-width: $t_{(51)} = 2.7280$, $p = 0.0087$; Threshold: $t_{(51)} = 0.8194$, $p = 0.4163$, unpaired Student's t test).

To directly characterize IHH training-associated activation of the DRN^{ePet1} neurons, we combined a viral genetic strategy with fiber photometry (Gunaydin et al., 2014) by expressing the genetically encoded Ca^{2+} indicator GCaMP6f (Chen et al., 2013) in DRN^{ePet1} neurons of free-moving *ePet1*-Cre mice (Fig. 5*D*). GCaMP6f expression and recording sites were verified by post hoc histology (Fig. 5*E*). Intriguingly, we found that DRN^{ePet1}

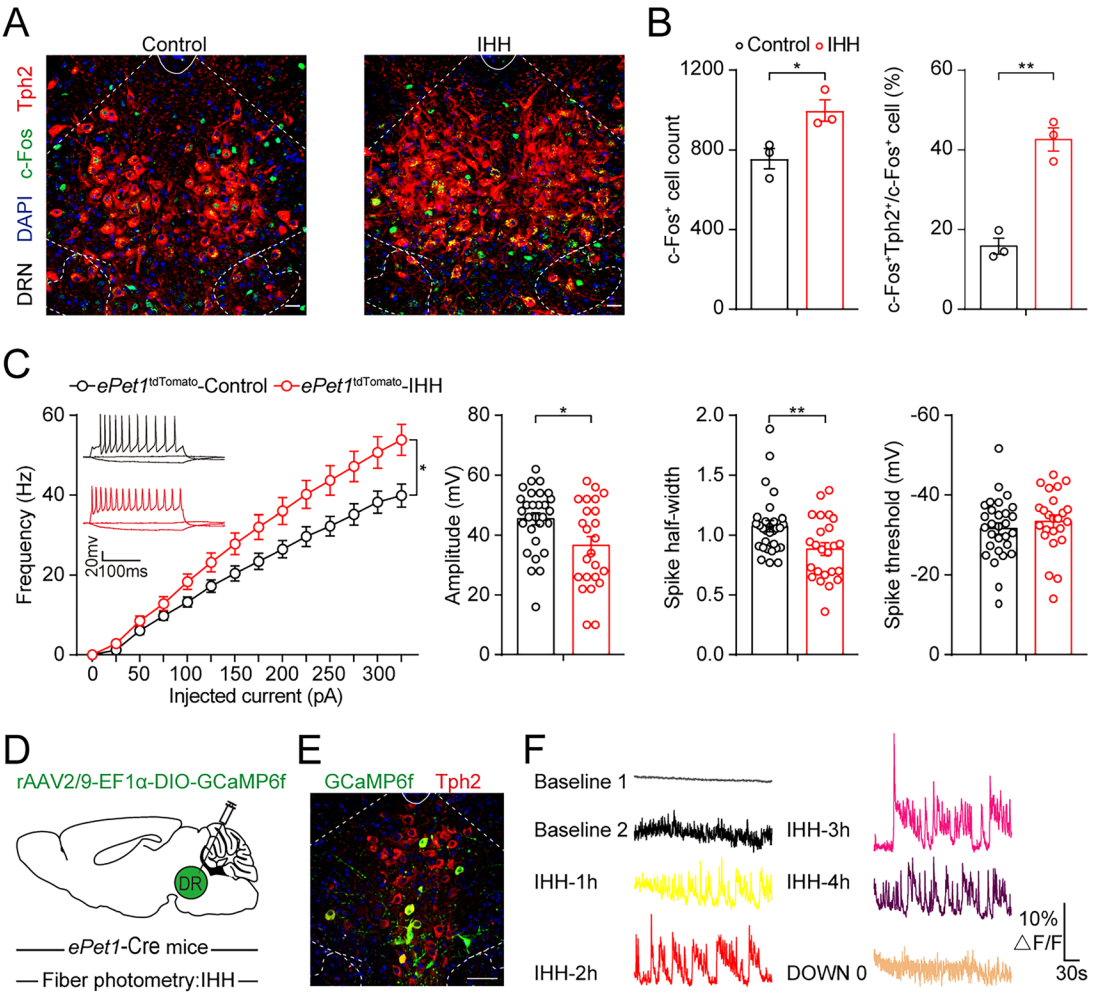

Figure 5. IHH activated serotonergic neurons in the DRN. ***A***, Representative confocal images of cells co-stained with anti-c-Fos and anti-Tph2 antibodies. ***B***, The number of c-Fos-positive cells and c-Fos/Tph2 double positive cells in the DRN of adult C57BL/6J mice treated with or without IHH ($n = 3$ mice per group). ***C***, Schematic diagram and statistics for serotonergic neuron action potentials in the DRN of *ePet1*^{tdTomato} mice following IHH treatment, compared to that of controls ($n = 29$–31 cells from 3 mice per group). ***D***, Schematic of the viral injection for expressing rAAV2/9-EF1α-DIO-GCaMP6f in DRN^{ePet1} neurons and optical fiber Ca^{2+} recordings during IHH training. ***E***, Representative images of GCaMP6f expression in Tph2-positive neurons in the DRN. ***F***, Calcium transients observed in DRN^{ePet1} neurons. Ca^{2+} imaging was performed during the first 5 min of each stage following IHH training (n = 2 mice). Scale bar = 50 µm. Data are presented as mean ± SEM. *$p < 0.05$, **$p < 0.01$, ***$p < 0.001$.

neurons were time-dependently activated during the IHH training paradigm, and the evoked activity persisted during the 4-h duration of IHH (Fig. 5*F*). Taken together, these results clearly showed that IHH training increased the activation of DRN^{ePet1} neurons, which contributed to the effect of IHH training and improved autistic-like phenotypes in mice.

DRN infusion of cobalt chloride alleviated autistic-like behaviors in *Shank3B*$^{-/-}$ mice

As we found that IHH training increased the expression of HIF1α in the DRN, we investigated whether it mediates the anti-autistic-like effect of IHH, and modulates the neuronal activity of DRN^{ePet1} neurons, using a pharmacological approach. Cobalt chloride ($CoCl_2$) is a chemical compound that mimics hypoxia at the biological level (Sulkshane et al., 2021; Kim et al., 2022). Consistently, we found that the protein level of HIF1α in the DRN of C57BL/6J mice significantly increased at 24 h after $CoCl_2$ infusion (Fig. 6*A,B*; $t_{(10)} = 4.2680$, $p = 0.0016$, unpaired Student's *t* test). Notably, infusion of $CoCl_2$ at a concentration of 200 μM did not induce neurotoxic effects. This was evidenced by the unaltered number of neurons in the DRN following $CoCl_2$ injection (Fig. 6*C,D*; $t_{(7)} = 1.2400$, $p = 0.2550$, unpaired Student's *t* test), and this is consistent with our previous report (Zhu et al., 2010).

Next, we microinjected $CoCl_2$ into the DRN of *Shank3B*$^{-/-}$ mice and control littermates, and conducted behavioral tests 24 h after the injection (Fig. 6*E*). We observed that the grooming time significantly increased in *Shank3B*$^{-/-}$ mice, compared to that in wild-type control littermates following vehicle injection. In contrast, infusion of $CoCl_2$ significantly decreased the duration of grooming in *Shank3B*$^{-/-}$ mice compared to that in vehicle-treated mutant mice (Fig. 6*F*; $F_{(1,\ 77)} = 9.2460$, $p = 0.0032$, interaction, $F_{(1,\ 77)} = 5.7820$, $p = 0.0186$, two-way ANOVA), and no significant difference in grooming time was observed in wild-type mice following $CoCl_2$ infusion. Moreover, in the three-chamber test, DRN infusion of $CoCl_2$ had little effect on social preference (Fig. 6*G,H*; *Shank3B*$^{+/+}$-Control: $F_{(2,57)} = 126.9800$, $p < 0.0001$; *Shank3B*$^{+/+}$-$CoCl_2$: $F_{(2,44)} = 49.0360$, $p < 0.0001$; *Shank3B*$^{-/-}$-Control: $F_{(2,54)} = 15.3270$, $p < 0.0001$; *Shank3B*$^{-/-}$-$CoCl_2$: $F_{(2,45)} = 22.1480$, $p < 0.0001$, one-way ANOVA), whereas $CoCl_2$ infusion reversed the deficits of social novelty in *Shank3B*$^{-/-}$ mice (Fig. 6*I,J*; *Shank3B*$^{+/+}$-Control: $F_{(2,57)} = 83.5570$, $p < 0.0001$; *Shank3B*$^{+/+}$-$CoCl_2$: $F_{(2,44)} = 68.4550$, $p < 0.0001$; *Shank3B*$^{-/-}$-Control: $F_{(2,54)} = 21.8920$, $p < 0.0001$; *Shank3B*$^{-/-}$-$CoCl_2$: $F_{(2,45)} = 56.6290$, $p < 0.0001$, one-way ANOVA). These results suggested that DRN infusion of $CoCl_2$ alleviated autistic-like behaviors in *Shank3B*$^{-/-}$ mice.

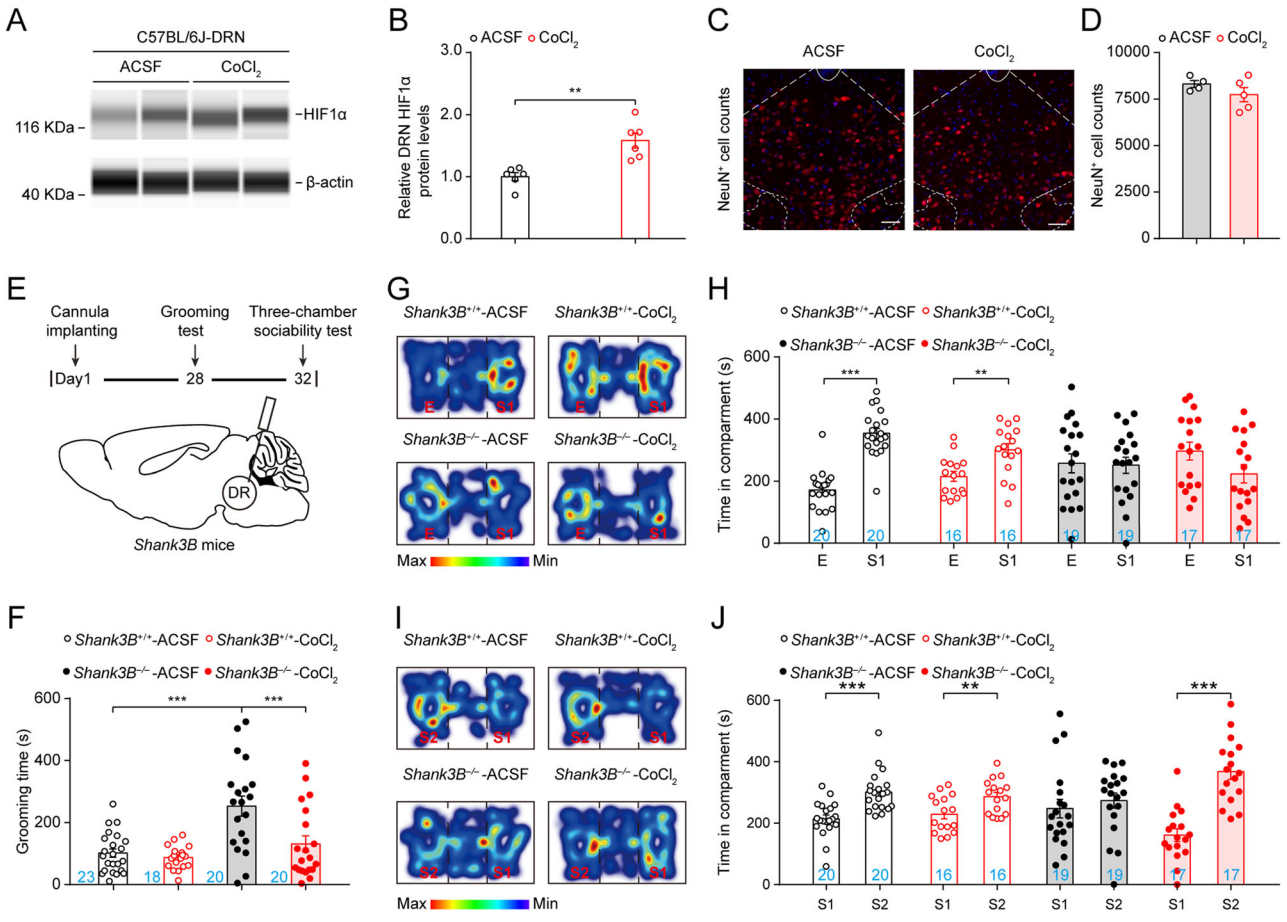

Figure 6. DRN infusion of cobalt chloride alleviated autistic-like behaviors in *Shank3B*$^{-/-}$ mice. ***A, B***, Relative HIF1α protein levels in the dorsal raphe nucleus (DRN) of C57BL/6J mice 24 h after treatment with $CoCl_2$ (200 μM) or artificial cerebrospinal fluid (ACSF) ($n = 6$ mice per group). ***C, D***, Representative images and statistics for anti-NeuN antibody staining in the DRN following DRN infusion of $CoCl_2$ or ACSF ($n = 4$–5 mice per group). ***E***, Schematic diagram of cannula insertion into the DRN of *Shank3B*$^{-/-}$ mice and behavioral tests. $CoCl_2$ (200 μM) was injected into the DRN 24 h before each behavioral test. ***F***, Grooming time ($n = 18$–23 mice per group). ***G–J***, The three-chamber sociality test ($n = 16$–20 mice per group). Scale bar = 50 μm. Data are presented as mean ± SEM. *$p < 0.05$, **$p < 0.01$, ***$p < 0.001$.

Knockdown of *Egln1* in the DRN^{ePet1} neurons rescued autistic-like phenotypes in *Shank3B*$^{-/-}$ mice

PHD2 is an oxygen sensor that negatively regulates HIF1α accumulation (Baik and Jain, 2020). To further characterize the role of HIF1α overexpression in DRN neurons, which contribute to the effect of IHH, we modulated HIF1α expression in DRN^{ePet1} neurons using a genetic approach. To validate our method, we microinjected either a Cre-dependent rAAV expressing *Egln1* short-hairpin RNA (shRNA) fused with green fluorescent protein (rAAV-hEF1a-DIO-EGFP-*Egln1*-shRNA, briefly *Egln1*-shRNA) or a control virus (SC) into the DRN of *ePet1*-Cre mice (Fig. 7*A*). As shown in Figure 7*B*, fluorescence of EGFP was observed only in the DRN, and the protein level of PHD2 was significantly decreased in the DRN of *ePet1*-Cre mice injected with *Egln1*-shRNA compared to that of mice injected with SC. As expected, *Egln1*-shRNA significantly increased HIF1α expression in the DRN (Fig. 7*C*,*D*; PHD2: $t_{(10)} = 3.6290$, $p = 0.0046$; HIF1α: $t_{(10)} = 3.2870$, $p = 0.0082$, unpaired Student's *t* test).

Next, we crossed *ePet1*-Cre mice with *Shank3B*$^{-/-}$ mice to obtain *Shank3B*$^{-/-}$-*ePet1*-Cre mice and their control littermates, *Shank3B*$^{+/+}$-*ePet1*-Cre mice. *Egln1*-shRNA or SC was microinjected into the DRN of these mice (Fig. 8*A*). Behavioral analysis showed that knockdown of PHD2 significantly decreased the grooming time in *Shank3B*$^{-/-}$ mice (Fig. 8*B*; $F_{(1,32)} = 10.7900$, $p = 0.0025$, interaction, $F_{(1,32)} = 8.1520$, $p = 0.0075$, two-way ANOVA) and restored the deficit social novel preference behaviors in *Shank3B*$^{-/-}$ mice, but had little effect on social preference behaviors (Fig. 8*C*–*F*; social preference, 8C, D: *Shank3B*$^{+/+}$-Control: $F_{(2,18)} = 31.1360$, $p < 0.0001$; *Shank3B*$^{+/+}$-*Egln1*-shRNA: $F_{(2,24)} = 50.0370$, $p < 0.0001$; *Shank3B*$^{-/-}$-Control: $F_{(2,27)} = 14.8370$, $p < 0.0001$; *Shank3B*$^{-/-}$-*Egln1*-shRNA: $F_{(2,24)} = 41.0460$, $p < 0.0001$; social novel preference, 8E, F: *Shank3B*$^{+/+}$-Control: $F_{(2,18)} = 33.0770$, $p < 0.0001$; *Shank3B*$^{+/+}$-*Egln1*-shRNA: $F_{(2,24)} = 11.8070$, $p = 0.0003$; *Shank3B*$^{-/-}$-Control: $F_{(2,27)} = 25.3650$, $p < 0.0001$; *Shank3B*$^{-/-}$-*Egln1*-shRNA: $F_{(2,24)} = 37.4350$, $p < 0.0001$, one-way ANOVA), indicating that overexpression of HIF1α in DRN^{ePet1} neurons ameliorated autistic-like behaviors in *Shank3B*$^{-/-}$ mice.

Next, we determined whether *Egln1* knockdown regulated the PSD protein levels in the striatum of *Shank3B*$^{-/-}$ mice. Western blotting showed that the downregulated protein levels of GluR2, NR2A, and NR2B in the striatum of *Shank3B*$^{-/-}$ mice were reversed by injecting *Egln1*-shRNA into the DRN, while knockdown of PHD2 in the DRN had little effect on these protein levels in wild-type animals (Fig. 8*G*,*H*; GluR1: $F_{(1,20)} = 3.3650$, $p = 0.0815$, interaction, $F_{(1,20)} = 1.004$, $p = 0.3284$; GluR2: $F_{(1,20)} = 1.2710$, $p = 0.2729$, interaction, $F_{(1,20)} = 4.0850$, $p = 0.0569$; NR2A: $F_{(1,20)} = 17.27$, $p = 0.0005$, interaction, $F_{(1,20)} = 19.9300$, $p = 0.0002$; NR2B: $F_{(1,20)} = 12.5600$, $p = 0.0020$, interaction, $F_{(1,20)} = 19.0900$, $p = 0.0003$, two-way ANOVA). Taken together, these results indicate that overexpression of HIF1α in DRN^{ePet1} neurons induced anti-autistic-like effects in *Shank3B*$^{-/-}$ mice.

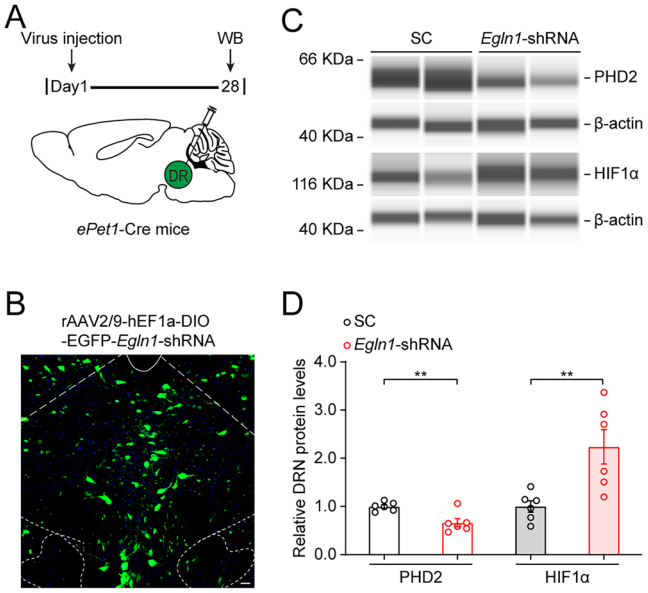

Figure 7. Validating the efficacy of *Egln1*-shRNA in the DRN of *ePet1*-Cre mice. ***A***, Schematic of viral injection. WB, western blot. ***B***, Representative images of EGFP expression in the dorsal raphe nucleus (DRN) of *ePet1*-Cre mice 28 d after the viral injection. ***C***, ***D***, Western blots analysis following DRN infusion of *Egln1*-shRNA or SC ($n = 6$ mice per group). Scale bar = 50 μm. Data are presented as mean ± SEM. $^{**}p < 0.01$.

Downregulation of PHD2 activated the DRN^{ePet1} neurons

We determined whether upregulation of HIF1α in DRN^{ePet1} neurons directly affects neuronal activity. To this end, mice were sacrificed after behavioral tests and brain slices containing the DRN were prepared. We found that the spontaneous firing rate of DRN^{ePet1} neurons in *Shank3B*$^{-/-}$ mice was lower than that in wild-type control animals. In contrast, knockdown of PHD2 significantly increased the firing rate of spontaneous action potentials of DRN^{ePet1} neurons in both *Shank3B*$^{-/-}$and wild-type mice, *Shank3B*$^{+/+}$, compared to their corresponding control mice (Fig. 9*A*,*B*; Frequency: $F_{(1,82)} = 44.4900$, $p < 0.0001$, interaction, $F_{(1,82)} = 1.8490$, $p = 0.0952$, two-way ANOVA). Moreover, we found that *Shank3* deletion decreased the firing rate and increased the spike half-width of depolarizing current-induced action potentials in DRN^{ePet1} neurons, without affecting the amplitude and spike threshold, compared with that in wild-type mice injected with SC. Intriguingly, knockdown of *Egln1* totally reversed the decreased firing rate and the increased spike half-width of depolarizing current-induced action potentials in DRN^{ePet1} neurons of *Shank3B*$^{-/-}$ mice, while downregulation of PHD2 also activated DRN^{ePet1} neurons in wild-type animals (Fig. 9*C*–*G*; frequency: $F_{(3,1296)} = 126.900$, $p < 0.0001$, interaction, $F_{(48,1296)} = 3.8540$, $p < 0.0001$, amplitude: $F_{(1,77)} = 9.9510$, $p = 0.0023$, interaction, $F_{(1,77)} = 0.2632$, $p = 0.6094$; half-width: $F_{(1,77)} = 21.9300$, $p < 0.0001$, interaction, $F_{(1,77)} = 3.2490$, $p = 0.0754$; threshold: $F_{(1,77)} = 14.3400$, $p = 0.0003$, interaction, $F_{(1,77)} = 0.1838$, $p = 0.6693$, two-way ANOVA). These results indicate that overexpression of HIF1α in DRN^{ePet1} neurons increased their neuronal excitability, and thus contributed to the anti-autistic-like effect of IHH.

Knockdown of Hif1α in DRN^{ePet1} neurons induced compulsive behaviors

To further establish the critical role of HIF1α signaling in DRN^{ePet1} neurons in autism-like phenotypes, we investigated whether downregulation of HIF1α induces autistic-like behaviors. To validate the efficiency of rAAV-CBG-DIO-EGFP-*Hif1a*-shRNA (referred to as *Hif1a*-shRNA), we injected rAAV-CMV-Cre and *Hif1a*-shRNA or SC into the DRN of C57BL/6J mice. All mice were sacrificed 4 weeks after virus injection (Fig. 10*A*,*B*). Western blot analysis showed that the protein level of HIF1α was significantly decreased in the DRN of mice injected with *Hif1a*-shRNA, compared to that of control animals injected with SC (Fig. 10*C*,*D*; $t_{(14)} = 3.9240$, $p = 0.0015$, unpaired

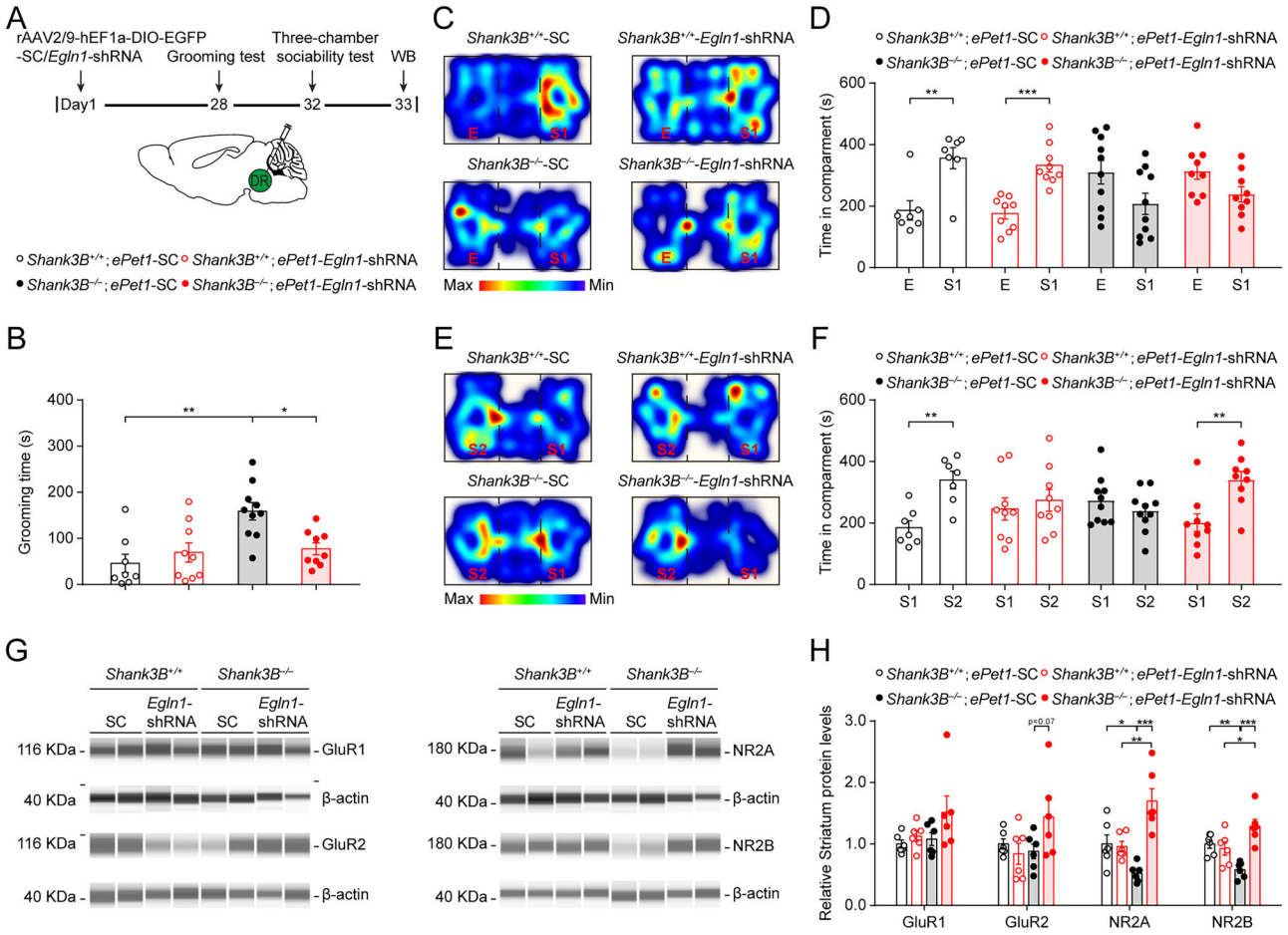

Figure 8. Knockdown of *Egln1* in the DRN^{ePet1} neurons rescued autistic-like phenotypes in *Shank3B*$^{-/-}$ mice. ***A***, Schematic of virus injection and behavioral tests. ***B***, Grooming time ($n = 8$–10 mice per group). ***C–F***, The three-chamber sociality test ($n = 8$–10 mice per group). ***G, H***, Western blotting for GluR1, GluR2, NR2A, and NR2B expression levels in the striatum of *Shank3B*$^{-/-}$ mice ($n = 6$ mice per group). Scale bar = 50 µm. Data are presented as mean ± SEM. $^{*}p < 0.05$, $^{**}p < 0.01$, $^{***}p < 0.001$.

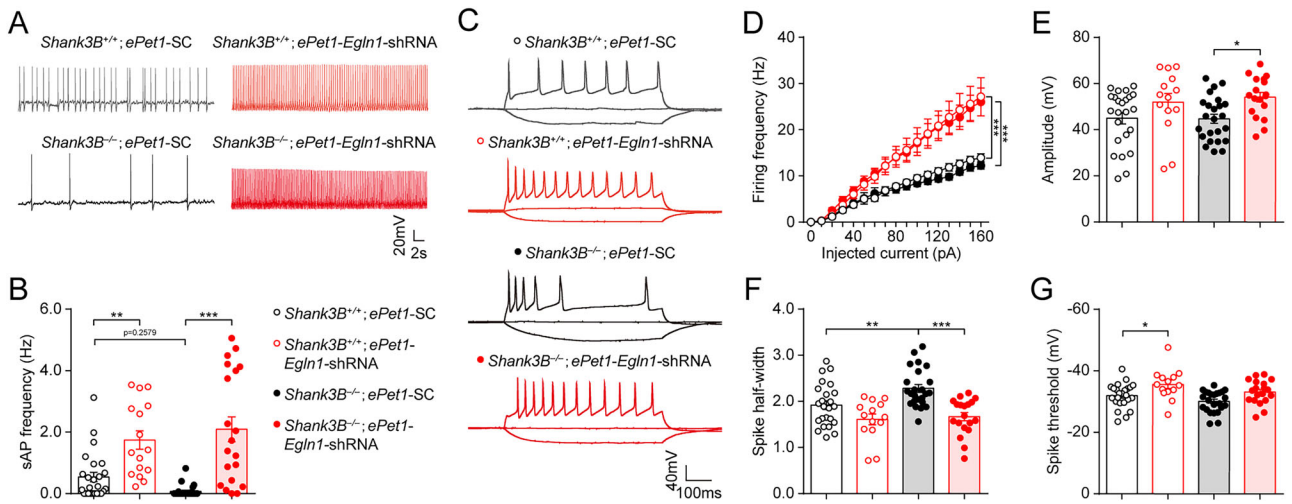

Figure 9. Downregulation of PHD2 activated the DRN^{ePet1} neurons of *Shank3B*$^{-/-}$ mice and wild-type littermates. ***A, B***, Prolyl hydroxylase domain-containing protein 2 (PHD2) knockdown increases the spontaneous action potential firing frequency of DR^{ePet1} neurons ($n = 16$–25 cells from 3 mice per group). ***C–G***, The effect of PHD2 knockdown on the firing rates, amplitudes, spike half-widths, and spike thresholds of depolarizing current-induced action potentials in DRN^{ePet1} neurons ($n = 14$–24 cells from 3 mice per group). Data are presented as mean ± SEM. $^{*}p < 0.05$, $^{**}p < 0.01$, $^{***}p < 0.001$.

Student's *t* test). Next, we microinjected *Hif1a*-shRNA or SC into the DRN of *ePet1*-Cre mice, and behavioral tests were conducted 4 weeks after virus injections (Fig. 11*A*,*B*). In the grooming test, knockdown of *Hif1a* in DRN^{ePet1} neurons significantly increased the time spent self-grooming, relative to that of control animals (Fig. 11*C*; $t_{(41)} = 2.3590$, $p = 0.0232$, unpaired Student's *t* test).

However, in the marble burying test, a slight difference was observed in the number of balls buried between the two groups, although the difference was not significant (Fig. 11*D*; $t_{(41)} = 1.209$, $p = 0.2336$, unpaired Student's t test). Knockdown of *Hif1a* in DRN^{ePet1} neurons had little effect on social preference (Fig. 11*E*,*F*; *ePet1*-Control: $F_{(2,69)} = 144.8990$, $p < 0.0001$; *ePet1*-sh*Hif1a*: $F_{(2,78)} = 155.1560$, $p < 0.0001$, one-way ANOVA) and social novel ability (Fig. 11*G*,*H*; *ePet1*-Control: $F_{(2,69)} = 38.8490$, $p < 0.0001$; *ePet1*-sh*Hif1a*: $F_{(2,78)} = 48.9960$, $p < 0.0001$, one-way ANOVA). A cell-attached voltage clamp was used to record the spontaneous firing activity of serotonergic neurons in DRN slices (Zou et al., 2020). Cell-attached voltage clamp recordings showed that knockdown of *Hif1a* in DRN^{ePet1} neurons decreased the firing rate of spontaneous firing activity (Fig. 12*A*,*B*; $t_{(57)} = 3.7320$, $p = 0.0004$, unpaired Student's t test) without affecting the firing frequency of depolarizing current-induced action potentials but increasing only the spike half-width (Fig. 12*C*–*E*; frequency: $F_{(1,644)} = 3.090$, $p = 0.0793$, two-way ANOVA; amplitude: $t_{(46)} = 1.4820$, $p = 0.1600$; half-width: $t_{(46)} = 3.8740$, $p = 0.0003$; threshold: $t_{(51)} = 0.2645$, $p = 0.7926$, unpaired Student's t test). These results support the notion that enhanced HIF1α signaling in DRN^{ePet1} neurons contributed to the anti-autistic-like effect of IHH.

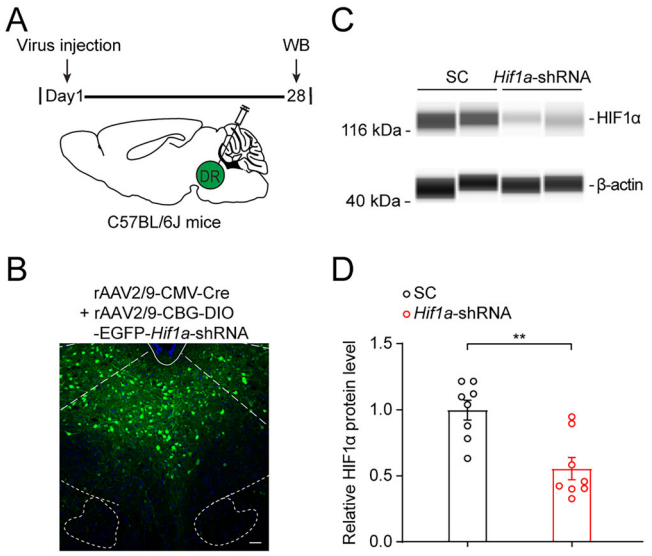

Figure 10. Validating the efficacy of *Hif1a*-shRNA in the DRN of C57BL/6J mice. ***A***, Schematic of virus injection. ***B***, Representative confocal images of EGFP expression 28 d after dorsal raphe nucleus (DRN) infusion of both rAAV-CMV-Cre and *Hif1a*-shRNA. ***C***, ***D***, Western blot assay showing that DRN infusion of both rAAV-CMV-Cre and *Hif1a*-shRNA significantly decreased the protein level of HIF1α in the DRN compared to that of mice injected with both rAAV-CMV-Cre and SC into the DRN ($n = 8$ mice per group). Scale bar = 50 µm. Data are presented as mean ± SEM. $^{**}p < 0.01$.

Discussion

In this study, we characterized the therapeutic potential of IHH in patients with ASD. The major discoveries were as follows: (1) IHH ameliorated autistic-like behaviors in two mouse models of ASD, *Shank3B*$^{-/-}$ and *Fmr1*$^{-/y}$ mice; (2) IHH activated serotonergic neurons in the DRN via enhancing HIF1α signaling; (3) upregulating the expression of HIF1α in DRN^{ePet1} neurons activated these neurons, improved autistic-like behaviors, and reversed the decreased expression of excitatory postsynaptic proteins in the striatum of *Shank3B*$^{-/-}$ mice; (4) downregulation of HIF1α in DRN^{ePet1} neurons decreased their excitability and induced compulsive behaviors in adult mice. These results suggest that IHH has potential to be a physical treatment option for ASD.

Previous studies have shown that autism is closely linked to synaptic dysfunction (Krueger et al., 2011; Peca et al., 2011; Xu et al., 2019; Zhang et al., 2019; Li and Pozzo-Miller, 2020; Jiang et al., 2022). Consistent with previous reports (Peca et al., 2011), we found that excitatory synaptic functions were disrupted in the two mouse models, showing that NR2A and NR2B expression was significantly decreased in the striatum of *Shank3B*$^{-/-}$ mice, and that the protein levels of GluR2, NR2A,

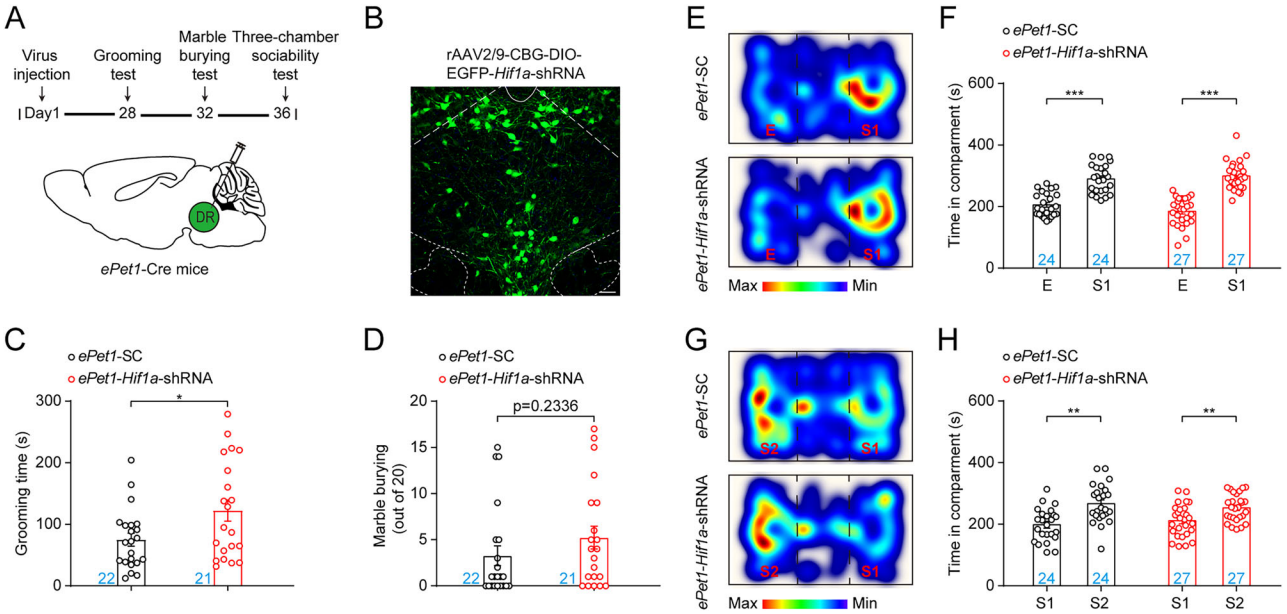

Figure 11. Knockdown of *Hif1a* in DRN^{ePet1} neurons induced compulsive behaviors. ***A***, ***B***, Schematic diagram of virus injection and behavioral tests. ***C***, Grooming test ($n = 21$–22 mice per group). ***D***, Marble burying test ($n = 21$–22 mice per group). ***E***–***H***, Three-chamber sociality test. ($n = 24$–27 mice per group). Data are presented as mean ± SEM. $^{*}p < 0.05$, $^{**}p < 0.01$, $^{***}p < 0.001$.

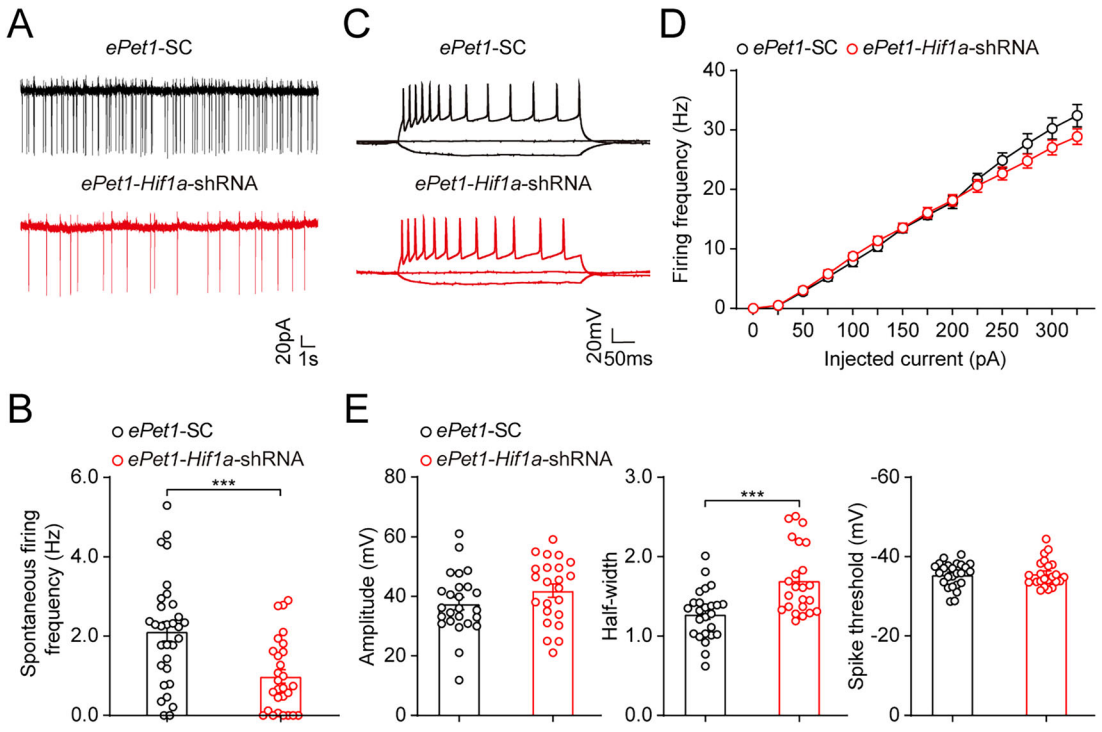

Figure 12. HIF1α knockdown in DRN^{ePet1} neurons reduced their spontaneous activity. ***A***, ***B***, HIF1α knockdown decreased the spontaneous firing frequency of DRN^{ePet1} neurons ($n = 28–31$ cells from 3 mice per group). ***C–E***, HIF1α knockdown had little effect on the firing rates, amplitudes, spike half-widths, and spike thresholds of depolarizing current-induced action potentials in DRN^{ePet1} neurons ($n = 23–25$ cells from 3 mice per group). Data are presented as mean ± SEM. ***$p < 0.001$.

and NR2B decreased in the mPFC of *Fmr1*$^{-/y}$ mice. We found that IHH training partially rescued the deficits in the expression of these PSD proteins, whereas the role of IHH on the expression of these PSD proteins differed in various brain regions, possibly because different brain region responding differently to hypoxia (Kawasaki et al., 1990; Zhu et al., 2010; Su et al., 2014; Mun et al., 2021). In addition, we observed that the protein levels of GluR2 were not significantly different between *Shank3B*$^{-/-}$ mice and their control littermates. These results were inconsistent with a previous report, possibly due to the age of the mice used (10–12-weeks old used in this study). Nevertheless, our data indicated that IHH training ameliorates synaptic dysfunction in ASD mouse models.

Serotonin neurons are closely involved in social behavior, and bidirectional modulation of DRN serotonin neuron activity modifies sociability (Luo et al., 2017; Walsh et al., 2018). In the present study, we found that the number of c-Fos-positive cells, especially the c-Fos/Tph2 dual-positive cells were significantly increased in the DRN after 14 d of IHH training. Moreover, using electrophysiological recordings, we found that IHH training significantly increased the firing rates of DRN^{ePet1} neurons. In addition, IHH training decreased the spike amplitude and half-width of action potentials without affecting the spike threshold, suggesting that modulation of sodium and/or potassium currents in response to IHH may underlie these electrophysiological alterations (Hempleman, 1995; Bean, 2007; Dizin et al., 2021). Using a calcium imaging approach, we observed that the frequency of Ca^{2+} transients increased dynamically increased during IHH processing. Furthermore, IHH training significantly increased HIF1α expression in DRN serotonergic neurons, and using pharmacological and genetic approaches, we found that overexpression of HIF1α increased spontaneous firing rates and the depolarizing current-induced action potentials of DRN^{ePet1} neurons. However, downregulation of HIF1α decreased the spontaneous firing rates, but did not influence the frequency of depolarizing current-induced action potentials. A previous study has shown that the cell-attached voltage-clamp mode is best-suited for recording spontaneous firing activity in the attached cells, whereas current-clamp recording is best-suited for recording synaptic events (Perkins, 2006; Zou et al., 2020). The spontaneous firing rates of DRN^{ePet1} neurons exhibited greater sensitivity compared to the action potentials induced by current injection following HIF1α knockdown. These results showed that IHH training enhanced the neuronal activity of serotonergic neurons in the DRN through upregulating HIF1α signaling, which contributes to the anti-autistic-like effect of IHH. Notably, it is of interest to determine how and why IHH training activates the serotonergic neurons in the DRN.

Limitations of the study

Clinical observations indicate that HIF1α contributes to the etiopathogenesis of ASD (Emanuele et al., 2010; Wang et al., 2021). In the present study, we found that IHH increased the expression of HIF1α, which may translocate into the nucleus of serotonergic neurons in the DRN and initiate a downstream signaling. Meanwhile, we found that knockdown of *Hif1α* in serotonergic neurons induced compulsive behaviors, whereas overexpressing HIF1α in these neurons significantly alleviated repetitive behaviors and social deficits in *Shank3B*$^{-/-}$ mice. These results suggest bidirectional modulation of autism-like behaviors by HIF1α signaling in serotonergic neurons. However, the specific set of downstream factors of HIF1α signaling remains unknown. One of the candidate factors is vascular endothelial growth factor (VEGF), another one could be erythropoietin (EPO). Clinical studies have shown that serum levels of VEGF are lower in patients with autism than in that of the control group

(Emanuele et al., 2010), whereas EPO treatment demonstrated beneficial effects on ASD-like symptoms in an lipopolysaccharide or valproate induced rat model of autism (Solmaz et al., 2020; Haratizadeh et al., 2023). Future studies are needed to investigate the downstream factors of HIF1α signaling, which may directly mediate the anti-autistic effects of IHH.

Another issue is the precise mode of the IHH. The effect of IHH is influenced by its mode. Hypoxia is a double-edged sword; the degree of hypoxia can play a protective role or damaging role. It has been shown that mild hypoxia (9–16% inspired O_2) generally produces beneficial effects without noticeable pathology, while severe hypoxia protocols (2–8% inspired O_2) induce pathological responses (Navarrete-Opazo and Mitchell, 2014). Studies have also shown that daily exposure to fewer than 15 cycles induces adaptive responses, whereas a higher frequency (48–2,400 episodes/d) can induce fatigue and discomfort, potentially leading to harm. Third, the difference between normobaric and hypobaric hypoxia may have influenced the effects of IHH. Intermittent normobaric hypoxia does not affect performance or erythropoietic markers in highly trained distance runners (Julian et al., 2004). In the present study, we performed IHH following our previously reported protocol of a 14-day IHH training at an altitude of 5000 m for 4 h per day, which did not show neurotoxicity in the adult brain (Zhu et al., 2010). However, a previous study showed that hypobaric and normobaric hypoxia elicited similar physiological responses (Richard and Koehle, 2012). Future experiments are required to optimize the mode of IHH, for example, to detect whether IHH at an altitude of 3,000 m for 3 h of training per day can ameliorate autistic-like phenotypes.

In summary, our results showed that IHH training at an altitude of 5,000 m, 4 h per day, for 14 consecutive days, produced anti-autistic-like effects in two mouse models of ASD via enhancing HIF1α signaling in the serotonergic neurons of the DRN, which resulted in their increased activity. These findings highlight the therapeutic potential of IHH in the treatment of ASD.

References

Ashley CT Jr, Wilkinson KD, Reines D, Warren ST (1993) FMR1 protein: conserved RNP family domains and selective RNA binding. Science 262:563–566.

Baik AH, Jain IH (2020) Turning the oxygen dial: balancing the highs and lows. Trends Cell Biol 30:516–536.

Barbosa-Silva MC, Campos RMP, Del Castilo I, Franca JV, Frost PS, Penido C, Clarke JR, Canetti C, Ribeiro-Resende VT (2022) Mice lacking 5-lipoxygenase display motor deficits associated with cortical and hippocampal synapse abnormalities. Brain Behav Immun 100:183–193.

Bean BP (2007) The action potential in mammalian central neurons. Nat Rev Neurosci 8:451–465.

Berry-Kravis EM, et al. (2018) Drug development for neurodevelopmental disorders: lessons learned from fragile X syndrome. Nat Rev Drug Discov 17:280–299.

Bilousova TV, Dansie L, Ngo M, Aye J, Charles JR, Ethell DW, Ethell IM (2009) Minocycline promotes dendritic spine maturation and improves behavioural performance in the fragile X mouse model. J Med Genet 46:94–102.

Bonkowsky JL, Son JH (2018) Hypoxia and connectivity in the developing vertebrate nervous system. Dis Model Mech 11(12):dmm037127.

Chen TW, et al. (2013) Ultrasensitive fluorescent proteins for imaging neuronal activity. Nature 499:295–300.

Darnell JC, et al. (2011) FMRP stalls ribosomal translocation on mRNAs linked to synaptic function and autism. Cell 146:247–261.

Dhamne SC, et al. (2017) Replicable in vivo physiological and behavioral phenotypes of the Shank3B null mutant mouse model of autism. Mol Autism 8:26.

DiCarlo GE, et al. (2019) Autism-linked dopamine transporter mutation alters striatal dopamine neurotransmission and dopamine-dependent behaviors. J Clin Invest 129:3407–3419.

Dizin E, et al. (2021) Activation of the hypoxia-inducible factor pathway inhibits epithelial sodium channel-mediated sodium transport in collecting duct principal cells. J Am Soc Nephrol 32:3130–3145.

Emanuele E, Orsi P, Barale F, di Nemi SU, Bertona M, Politi P (2010) Serum levels of vascular endothelial growth factor and its receptors in patients with severe autism. Clin Biochem 43:317–319.

Ergaz Z, Weinstein-Fudim L, Ornoy A (2016) Genetic and non-genetic animal models for autism spectrum disorders (ASD). Reprod Toxicol 64: 116–140.

Goddard AW, Shekhar A, Whiteman AF, McDougle CJ (2008) Serotoninergic mechanisms in the treatment of obsessive-compulsive disorder. Drug Discov Today 13:325–332.

Gunaydin LA, et al. (2014) Natural neural projection dynamics underlying social behavior. Cell 157:1535–1551.

Hagerman RJ, et al. (2017) Fragile X syndrome. Nat Rev Dis Primers 3:17065.

Haratizadeh S, Ranjbar M, Darvishzadeh-Mahani F, Basiri M, Nozari M (2023) The effects of postnatal erythropoietin and nano-erythropoietin on behavioral alterations by mediating K-Cl co-transporter 2 in the valproic acid-induced rat model of autism. Dev Psychobiol 65:e22353.

Hempleman SC (1995) Sodium and potassium current in neonatal rat carotid body cells following chronic in vivo hypoxia. Brain Res 699:42–50.

Herbert MR (2011) SHANK3, the synapse, and autism. N Engl J Med 365: 173–175.

Herrera DG, Robertson HA (1996) Activation of c-fos in the brain. Prog Neurobiol 50:83–107.

Hirota T, King BH (2023) Autism spectrum disorder: a review. JAMA 329: 157–168.

Jacobsen JP, Siesser WB, Sachs BD, Peterson S, Cools MJ, Setola V, Folgering JH, Flik G, Caron MG (2012) Deficient serotonin neurotransmission and depression-like serotonin biomarker alterations in tryptophan hydroxylase 2 (Tph2) loss-of-function mice. Mol Psychiatry 17: 694–704.

Jiang CC, Lin LS, Long S, Ke XY, Fukunaga K, Lu YM, Han F (2022) Signalling pathways in autism spectrum disorder: mechanisms and therapeutic implications. Signal Transduct Target Ther 7:229.

Julian CG, Gore CJ, Wilber RL, Daniels JT, Fredericson M, Stray-Gundersen J, Hahn AG, Parisotto R, Levine BD (2004) Intermittent normobaric hypoxia does not alter performance or erythropoietic markers in highly trained distance runners. J Appl Physiol (1985) 96:1800–1807.

Kalueff AV, Aldridge JW, LaPorte JL, Murphy DL, Tuohimaa P (2007) Analyzing grooming microstructure in neurobehavioral experiments. Nat Protoc 2:2538–2544.

Kawasaki K, Traynelis SF, Dingledine R (1990) Different responses of CA1 and CA3 regions to hypoxia in rat hippocampal slice. J Neurophysiol 63:385–394.

Kazdoba TM, Leach PT, Yang M, Silverman JL, Solomon M, Crawley JN (2016) Translational mouse models of autism: advancing toward pharmacological therapeutics. Curr Top Behav Neurosci 28:1–52.

Kim GH, et al. (2018) Hypothalamic ER-associated degradation regulates POMC maturation, feeding, and age-associated obesity. J Clin Invest 128:1125–1140.

Kim SR, Seong KJ, Kim WJ, Jung JY (2022) Epigallocatechin gallate protects against hypoxia-induced inflammation in microglia via NF-kappaB suppression and Nrf-2/HO-1 activation. Int J Mol Sci 23:4004.

Krueger DD, Osterweil EK, Chen SP, Tye LD, Bear MF (2011) Cognitive dysfunction and prefrontal synaptic abnormalities in a mouse model of fragile X syndrome. Proc Natl Acad Sci U S A 108:2587–2592.

Li Q, et al. (2021) HIF-1alpha-induced expression of m6A reader YTHDF1 drives hypoxia-induced autophagy and malignancy of hepatocellular carcinoma by promoting ATG2A and ATG14 translation. Signal Transduct Target Ther 6:76.

Li W, Pozzo-Miller L (2020) Dysfunction of the corticostriatal pathway in autism spectrum disorders. J Neurosci Res 98:2130–2147.

Lipkin WI, Bresnahan M, Susser E (2023) Cohort-guided insights into gene-environment interactions in autism spectrum disorders. Nat Rev Neurol 19:118–125.

Liu Z, et al. (2014) Dorsal raphe neurons signal reward through 5-HT and glutamate. Neuron 81:1360–1374.

Lord C, et al. (2022) The lancet commission on the future of care and clinical research in autism. Lancet 399:271–334.

Lu XJ, Chen XQ, Weng J, Zhang HY, Pak DT, Luo JH, Du JZ (2009) Hippocampal spine-associated Rap-specific GTPase-activating protein induces enhancement of learning and memory in postnatally hypoxia-exposed mice. Neuroscience 162:404–414.

Luo J, Feng Q, Wei L, Luo M (2017) Optogenetic activation of dorsal raphe neurons rescues the autistic-like social deficits in Shank3 knockout mice. Cell Res 27:950–953.

Mun B, Jang YC, Kim EJ, Kim JH, Song MK (2021) Brain activity after intermittent hypoxic brain condition in rats. Brain Sci 12:52.

Navarrete-Opazo A, Mitchell GS (2014) Therapeutic potential of intermittent hypoxia: a matter of dose. Am J Physiol Regul Integr Comp Physiol 307: R1181–R1197.

Neubauer JA (2001) Invited review: physiological and pathophysiological responses to intermittent hypoxia. J Appl Physiol (1985) 90:1593–1599.

Paxinos G, Franklin KBJ (2004) *The mouse brain in stereo-taxic coordinates*. 3rd ed. San Diego, CA: Aca-demic Press.

Peca J, Feliciano C, Ting JT, Wang W, Wells MF, Venkatraman TN, Lascola CD, Fu Z, Feng G (2011) Shank3 mutant mice display autistic-like behaviours and striatal dysfunction. Nature 472:437–442.

Perkins KL (2006) Cell-attached voltage-clamp and current-clamp recording and stimulation techniques in brain slices. J Neurosci Methods 154:1–18.

Rein B, Ma K, Yan Z (2020) A standardized social preference protocol for measuring social deficits in mouse models of autism. Nat Protoc 15: 3464–3477.

Richard NA, Koehle MS (2012) Differences in cardio-ventilatory responses to hypobaric and normobaric hypoxia: a review. Aviat Space Environ Med 83:677–684.

Russo SJ, Murrough JW, Han MH, Charney DS, Nestler EJ (2012) Neurobiology of resilience. Nat Neurosci 15:1475–1484.

Schodel J, Ratcliffe PJ (2019) Mechanisms of hypoxia signalling: new implications for nephrology. Nat Rev Nephrol 15:641–659.

Scott MM, Wylie CJ, Lerch JK, Murphy R, Lobur K, Herlitze S, Jiang W, Conlon RA, Strowbridge BW, Deneris ES (2005) A genetic approach to access serotonin neurons for in vivo and in vitro studies. Proc Natl Acad Sci U S A 102:16472–16477.

Semenza GL (2012) Hypoxia-inducible factors in physiology and medicine. Cell 148:399–408.

Serebrovskaya TV, Xi L (2016) Intermittent hypoxia training as non-pharmacologic therapy for cardiovascular diseases: practical analysis on methods and equipment. Exp Biol Med (Maywood) 241:1708–1723.

Solmaz V, Erdogan MA, Alnak A, Meral A, Erbas O (2020) Erythropoietin shows gender dependent positive effects on social deficits, learning/memory impairments, neuronal loss and neuroinflammation in the lipopolysaccharide induced rat model of autism. Neuropeptides 83:102073.

Su J, Wang W, Sun L, Li T, Kong D, Kang J (2014) Raphe serotonergic neurons modulate genioglossus corticomotor activity in intermittent hypoxic rats. Respir Res 15:76.

Sulkshane P, Ram J, Thakur A, Reis N, Kleifeld O, Glickman MH (2021) Ubiquitination and receptor-mediated mitophagy converge to eliminate oxidation-damaged mitochondria during hypoxia. Redox Biol 45:102047.

Sun C, Fu J, Qu Z, Jia L, Li D, Zhen J, Wang W (2020) Chronic intermittent hypobaric hypoxia restores hippocampus function and rescues cognitive impairments in chronic epileptic rats via Wnt/β-catenin signaling. Front Mol Neurosci 13:617143.

Trost B, et al. (2022) Genomic architecture of autism from comprehensive whole-genome sequence annotation. Cell 185:4409–4427 e4418.

Varghese M, et al. (2017) Autism spectrum disorder: neuropathology and animal models. Acta Neuropathol 134:537–566.

Viscor G, Torrella JR, Corral L, Ricart A, Javierre C, Pages T, Ventura JL (2018) Physiological and biological responses to short-term intermittent hypobaric hypoxia exposure: from sports and mountain medicine to new biomedical applications. Front Physiol 9:814.

Walsh JJ, Christoffel DJ, Heifets BD, Ben-Dor GA, Selimbeyoglu A, Hung LW, Deisseroth K, Malenka RC (2018) 5-HT release in nucleus accumbens rescues social deficits in mouse autism model. Nature 560:589–594.

Wang CS, Kavalali ET, Monteggia LM (2022) BDNF signaling in context: from synaptic regulation to psychiatric disorders. Cell 185:62–76.

Wang W, Tang J, Zhong M, Chen J, Li T, Dai Y (2021) HIF-1 alpha may play a role in late pregnancy hypoxia-induced autism-like behaviors in offspring rats. Behav Brain Res 411:113373.

Willsey HR, Willsey AJ, Wang B, State MW (2022) Genomics, convergent neuroscience and progress in understanding autism spectrum disorder. Nat Rev Neurosci 23:323–341.

Xia X, Lemieux ME, Li W, Carroll JS, Brown M, Liu XS, Kung AL (2009) Integrative analysis of HIF binding and transactivation reveals its role in maintaining histone methylation homeostasis. Proc Natl Acad Sci U S A 106:4260–4265.

Xu P, Chen A, Li Y, Xing X, Lu H (2019) Medial prefrontal cortex in neurological diseases. Physiol Genomics 51:432–442.

Zhang K, et al. (2017) Elevated progranulin contributes to synaptic and learning deficit due to loss of fragile X mental retardation protein. Brain 140: 3215–3232.

Zhang JX, Chen XQ, Du JZ, Chen QM, Zhu CY (2005) Neonatal exposure to intermittent hypoxia enhances mice performance in water maze and 8-arm radial maze tasks. J Neurobiol 65:72–84.

Zhang XC, Shu LQ, Zhao XS, Li XK (2019) Autism spectrum disorders: autistic phenotypes and complicated mechanisms. World J Pediatr 15:17–25.

Zhou Y, et al. (2019) Atypical behaviour and connectivity in SHANK3-mutant macaques. Nature 570:326–331.

Zhu XH, et al. (2010) Intermittent hypoxia promotes hippocampal neurogenesis and produces antidepressant-like effects in adult rats. J Neurosci 30: 12653–12663.

Zou WJ, et al. (2020) A discrete serotonergic circuit regulates vulnerability to social stress. Nat Commun 11:4218.